ACOUSTIC EMISSION-BASED SENSOR ANALYSIS AND DAMAGE CLASSIFICATION FOR STRUCTURAL HEALTH MONITORING OF COMPOSITE STRUCTURES

by

Bibhisha Uprety

A thesis submitted to the faculty of
The University of Utah
in partial fulfillment of the requirements for the degree of

Master of Science

Department of Mechanical Engineering

The University of Utah

May 2015

The University of Utah Graduate School

STATEMENT OF THESIS APPROVAL

The following faculty members served as the supervisory committee chair and members for the thesis of Bibhisha Uprety. Dates at right indicate the members' approval of the thesis.

Daniel O. Adams, Chair	03/13/2015 Date Approved
V. John Mathews, Member	03/13/2015 Date Approved
Christopher Deemer, Member	03/13/2015 Date Approved

The thesis has also been approved by Tim Ameel, Chair of the Department/School/College of Mechanical Engineering and by David Kieda, Dean of The Graduate School.

ABSTRACT

Within the aerospace industry the need to detect and locate impact events, even when no visible damage is present, is important both from the maintenance and design perspectives. This research focused on the use of Acoustic Emission (AE) based sensing technologies to identify impact events and characterize damage modes in composite structures for structural health monitoring. Six commercially available piezoelectric AE sensors were evaluated for use with impact location estimation algorithms under development at the University of Utah. Both active and passive testing were performed to estimate the time of arrival and plate wave mode velocities for impact location estimation. Four sensors were recommended for further comparative investigations. Furthermore, instrumented low-velocity impact experiments were conducted on quasi-isotropic carbon/epoxy composite laminates to initiate specific types of damage: matrix cracking, delamination and fiber breakage. AE signal responses were collected during impacting and the test panels were ultrasonically C-scanned after impact to identify the internal damage corresponding to the AE signals. Matrix cracking and delamination damage produced using more compliant test panels and larger diameter impactor were characterized by lower frequency signals while fiber breakage produced higher frequency responses. The results obtained suggest that selected characteristics of sensor response signals can be used both to determine whether damage is produced during impacting and to characterize the types of damage produced in an impacted composite structure.

TABLE OF CONTENTS

LIST OF TABLES

LIST OF FIGURES

ACKNOWLEDGEMENTS

This work is supported in part by the National Aeronautics and Space Administration (Award No. NNM13AA12G) and the Air Force Office of Scientific Research (Award No. FA95501210291).

I would like to extend my deepest gratitude to everyone who assisted me in my efforts to successfully receive a Master of Science degree at the University of Utah.

I am very grateful to Dr. Dan Adams, my advisor and my mentor, for believing in me and providing me unparalleled support and encouragement throughout the project. I am thankful for his insights and guidance, and moreover his confidence in me to execute the research as I found suitable. I would also like to express my sincere thanks to Dr. V. John Mathews, my co-advisor, for his time and honesty, his willingness to advise me on fields out of my expertise and his constructive observations on the work.

I would like to thank Dr. Chris Deemer, a member of my committee, for sharing his knowledge and expertise and for expressing interest in my research. I really appreciate his time and patience with our test methods and constant encouragement throughout. His expert opinion and advice are much valued.

I wish to thank all the people involved in this project for their guidance and support in making this a success: Dr. Joel Harley for his keen interest and advising; Jeff Kessler for all the laboratory assistance, sharing ideas and opinions and moreover, investing in proper execution of all lab work for this project. I owe thanks to all the co-workers in this

project for helpful insights and comments during meetings and analysis. Sincere gratitude goes out to Sungwon Kim, for assisting me in design and fabrication of composite panels as well as experimental testing and analysis. I am grateful to all the graduate and undergraduate students at the Composites lab for training and providing assistance every time I needed it.

I owe sincere gratitude to Alan Done at Salt Lake Community College (SLCC) and David Sligar at Davis Applied Technology College (DATC) who cooperated and coordinated throughout my research work for all design and fabrications and making their lab available for use.

At last, this would not have been successful without the constant love and support of my family and friends. Much respect and gratitude to them for teaching me to believe in my dreams and working hard to ensure my education gets completed without any adversities.

CHAPTER 1

INTRODUCTION

1.1 Background

Due to their lighter weight, higher strength-to-weight and stiffness-to-weight ratio, fiber-reinforced composites are quickly getting popular in aerospace and aircraft as well as other manufacturing industries. As a result, composites are proving to be an effective alternative to using traditional metals such as aluminum, steel and titanium (Diamanti & Soutis, 2010). In the case of Space Launch System (SLS) structures, the light-weight composites that can be easily fabricated to form intricate shapes allow easier as well as economical manufacturing. However, the anisotropic material properties and heterogeneous microstructure of such fiber-reinforced composite materials make them a complex study and internal damage and failure modes may be produced without prior knowledge. Damage modes such as delaminations, fiber breakage and matrix cracking could significantly reduce the strength, durability and stability of the structure. These damage events especially due to low-velocity impacts are difficult to detect and could lead to catastrophic failures if not mitigated on time (Diamanti & Soutis, 2010). Hence, the purpose of this study is to identify the occurrence of such damage modes that initiate due to an unknown low-velocity impact event. In doing so, Acoustic Emission (AE) piezoelectric sensors are used to understand the material response to such events that help

in damage identification and characterization for effective structural health monitoring. The process of Structural Health Monitoring (SHM) provides constant screening of composite structures to identify any damage produced in the structure. In contrast to conventional Non-Destructive Inspection (NDI) techniques, SHM additionally allows real-time in-situ inspection of composite structures thereby reducing downtime as well as maintenance costs (Kessler et.al, 2002). To do so, experimental test conditions are simulated to understand the damage modes as well as the extent of damage expected in SLS structures. Such knowledge of material behavior with impact type events could provide mitigating solutions via design modifications to enable better logistics and a higher factor of safety (Giurgiutiu et. al, 2002).

There are a number of NDI techniques in use such as visual inspections, ultrasonic inspections, eddy current inspections, and thermography. The reliability of each technique is dependent on the expertise of the individuals performing these inspections (Giurgiutiu et. al, 2002). In addition, such inspections require significant downtime to examine the structure and identify damage locations. As a result, AE-based SHM systems are of interest due to their ability to provide real-time monitoring of large areas of structures with minimal intrusion to the component (Prosser et. al, 1999). The use of the piezoelectric sensor network allows inspection of larger areas of these structures and guided waveform analysis can help detect, localize, and assess the extent of damage type due to an unknown impact event (Giurgiutiu et. al, 2002).

1.1.1 Lamb Wave Theory

Acoustic Emissions are the stress waves that are generated as a material response to an external impact. Horace Lamb in 1917 mathematically proved the presence of mechanical stress waves that propagate in a structure guided by two parallel closed boundaries, referred to as guided or Lamb waves. Such Lamb waves can propagate through larger distances with smaller waveform amplitude attenuation (Prosser et. al, 1999).

For a test structure, Classical Plate Theory (CLT) considers two basic modes of Lamb wave propagation, namely the symmetric extensional (S) and asymmetric flexural (A) modes. A thin-plate structure at a lower frequency of excitation contains Lamb waves limited to the first symmetric (S_o) and the first asymmetric (A_o) modes (Prosser et. al, 1991). While the S_o mode is a longitudinal compression-traction mode, the A_o mode is primarily a transverse bending mode, generating deformation mostly in the thickness direction, as shown in Figure 1.1. Higher-order Lamb waves, identified by S_n or A_n ($n = 1, 2 \ldots$) exist for higher frequency inputs and thicker laminates exhibiting dispersion of wave mode propagation (Papulak, 2012).

Both symmetric and asymmetric wave modes contain in-plane and out-of-plane displacement components. However, the symmetric (extensional) mode consists primarily of in-plane displacements in the direction of wave propagation while the asymmetric (flexural) mode is primarily out-of-plane displacements normal to the direction of wave propagation as shown in Figure 1.1. These two-dimensional elastic stress waves propagate dispersively in the plane of the plate through the cross-sectional area (Papulak, 2012). In terms of waveform propagation, low-velocity impacts predominantly produce flexural

plate mode propagation while the extensional plate wave mode is much larger in high velocity impact events (Papulak, 2012).

Two types of AE-based systems are of interest for use in SHM of composite structures: active systems and passive systems. While active testing is mostly effective for a known damage source, passive systems are primarily chosen for their applicability to localize and detect damage caused by an unknown impact event. Additionally, passive testing allows for real-time impact conditions such as pencil-lead break, STEEL BALL drop and low-velocity impact testing as opposed to active testing that uses a transducer to send out an excitation signal further received by a sensor array (Grosse & Ohtsu, 2008). When damage is initiated, strain energy is released and passive testing allows for monitoring of this energy propagation in the structure. For an AE-based SHM study, it is, however, important to distinguish between damage related events and noise propagation.

Of the many sensor types that are of use in AE studies, piezoelectric sensors are commonly used for studying Lamb waves due to their low profile and operating frequencies. As the name suggests, the sensors in use have a piezoelectric sensing element that generates a charge response upon impact. Such sensors can be used both as actuating transducers and receivers for AE analysis (Giurgiutiu, 2002). By the use of such piezoelectric sensors for AE-based SHM systems, waveform transmissions can be recorded and analyzed, thereby identifying any changes to the received signal that could indicate damage events.

1.1.2 Impact Testing

There are various types of low-velocity impact tests that may be performed in a laboratory setting, such as Charpy impact testing, Izod impact testing, and instrumented drop weight impact testing. For an impact test to be considered "low-velocity" the impactor velocity should be lower than 100 m/s (Mallick, 1997). For many applications of composite structures, low-velocity impacts are a significant concern, ranging from tool drops, hail strike, and fly-away debris impacts. Both Charpy and Izod impact testing employ the use of a swinging pendulum to initiate an impact event, and input velocity and energy values are prescribed through the selection of drop height and impacting mass (Mallick, 1997). In contrast, instrumented drop tower testing is typically more representative of a real-life impact event. An instrumented impactor tup with the desired mass is dropped from a prescribed height onto a test specimen to create the desired impact event (Richardson & Wisheart, 1996).

For impact velocities less than 10 m/s, the response of the plate is determined primarily by the impactor/plate mass ratio rather than the impactor velocity. The contact duration of the impactor with the test structure allows the entire structure to absorb higher elastic energy causing a quasi-static response (Richardson & Wisheart, 1996). Damage modes are highly dependent on the material thickness, stiffness and boundary conditions for low-velocity impact experiments. The impact energy for a compliant boundary condition is mainly absorbed in the form of strain energy, but also by damage initiation and frictional losses (Richardson & Wisheart, 1996).

For low-velocity impacts of relatively compliant composite structures by blunt impactor, the damage created in the composite is typically matrix cracking followed by

delamination at the lamina interfaces. For a more compliant thin composite plate, matrix cracking usually propagates through a series of intraply cracking, leading to interfacial delaminations (Mal, 2003). The support conditions used in such impacts directly affect the size and area of the damaged region in or around the impacting projectile (Mal, 2003).

1.1.3 Failure Modes in Composites

There are three primary failure types that can occur in composite structures: matrix cracking, delamination and fiber breakage (Davies & Zhang, 1995). Matrix cracking is usually the first failure mode to be produced from a low-velocity impact. This type of damage is produced when the matrix material (typically an epoxy) cracks without breaking the surrounding fibers. Such matrix cracks are oriented parallel to the reinforcing fibers, and often follow the fiber/matrix interface. Although matrix cracking is often considered not to be critical to the integrity of a composite structure, this form of damage can lead to other failure modes, particularly delamination (Richardson & Wisheart, 1996). Delamination is one of the common failure modes that occurs in fiber-reinforced composite laminates, and is typically defined as a "separation at the ply-boundary" (Davies & Zhang, 1995). Interlaminar shear and normal stresses commonly produced by out-of-plane loading area are the common cause of delaminations in laminated composites. Fiber breakage occurs due to locally induced high stresses and indentation effects (Davies & Zhang, 1995).

Of the targeted damage states, fiber breakage with minimal matrix cracking and delamination can be achieved using a thicker laminate, a back-face supported test condition and a more pointed impactor. On the other hand, matrix cracking and delamination with minimal fiber breakage can be obtained using a thinner laminate, a larger diameter

impactor (cylindrical or spherical) and compliant boundary conditions that allow global structural deformations.

1.2 Objectives

As part of a larger research investigation focusing on AE-based structural health monitoring of composite structures, the primary objectives of this study are:

1. To identify suitable AE sensor types for initial time of arrival estimation and representative plate wave mode analysis for impact location estimation.
2. To identify damage producing impact events and perform damage characterization based on the waveform analysis.

1.3 Thesis Organization

Acoustic Emission-based Structural Health Monitoring requires the use of a piezoelectric sensor network attached to the outside of the structures to record impact events. Use of a proper sensor network is therefore imperative for impact location estimation and damage classification, which are discussed in the following chapters. A comparative analysis of various piezoelectric sensor types is presented in Chapter 2. Various testing methods involved in the evaluation such as active and passive testing are discussed and a recommendation is made for sensors to be used in impact location estimation. Chapter 3 presents the low-velocity impact experiments performed on composite structures for AE-based damage identification and classification. Finally in Chapter 4, a brief summary of the results and the findings are presented and potential future research directions are discussed.

1.4 References

Davies, G. A., & Zhang, X. (1995). Impact damage prediction in carbon composite structures. *International Journal of Impact Engineering*, *6*(11), 149-170.

Diamanti, K., & Soutis, C. (2010). Structural health monitoring techniques for aircraft composite structures. *Progress in Aerospace Sciences*, *46*(8), 342-352.

Giurgiutiu, V., Zagrai, A., & Bao, J. J. (2002). Piezoelectric wafer embedded active sensors for aging aircraft structural health monitoring. *Structural Health Monitoring-an International Journal*, *1*(1), 41-61.

Grosse, C. U., & Ohtsu, M. (2008). Introduction. In *Acoustic emission testing: Basics for research, applications in civil engineering* (pp. 3-6). Berlin: Springer.

Kessler, S. S., Spearing, S. M., & Soutis, C. (2002). Damage detection in composite materials using lamb wave methods. *Smart Materials & Structures*, *11*(2), 269-278.

Mal, A. K., Shih, F., & Banerjee, S. (2003). Acoustic emission waveforms in composite laminates under low-velocity impact. *Proc. SPIE 5047, Smart Nondestructive Evaluation and Health Monitoring of Structural and Biological Systems II,* 1-12.

Mallick, P. K. (1997). Laminate polymer matrix composites. In *Composites engineering handbook* (pp. 848-851). New York. CRC Press.

Papulak, T. S. (2012). *An inverse acoustical phased array technique for impact detection and location* (Master's thesis, University of Utah).

Prosser, W. H., Gorman, M. R., & Humes, D. H. (1999). Acoustic emission signals in thin plates produced by impact damage. *Journal of Acoustic Emission*, *17*(1-2), 29-36.

Prosser, W. H. (1991). *The propagation characteristics of the plate modes of acoustic emission waves in thin aluminum lates and thin graphite/epoxy composite plates and tubes* (Doctoral dissertation, John Hopkins University).

Richardson, M. O., & Wisheart, M. J. (1996). Review of low-velocity impact properties of composite materials. *Composites part a-applied science and manufacturing*, *27*(12), 1123-1131.

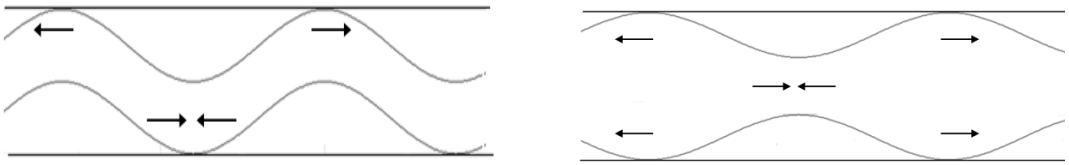

(a) **(b)**

Figure 1.1. Two Modes of Wave Propagation (a) Asymmetric (b) Symmetric.

CHAPTER 2

A COMPARATIVE EVALUATION OF PIEZOELECTRIC SENSORS FOR ACOUSTIC EMISSION-BASED IMPACT LOCATION ESTIMATION AND DAMAGE CLASSIFICATION IN COMPOSITE STRUCTURES

2.1 Abstract

Acoustic Emission (AE) based Structural Health Monitoring (SHM) is of great interest for detecting impact damage in composite structures. Within the aerospace industry the need to detect and locate these events, even when no visible damage is present, is important both from the maintenance and design perspectives. In this investigation, six commercially available piezoelectric sensors were evaluated for usage in an AE-based SHM system. Of particular interest was comparing the acoustic response of the candidate piezoelectric sensors for impact location estimations in fiber-reinforced composite structures. Sensor assessment was performed based on response signal characterization and performance for active testing at 300 kHz and steel-ball drop testing using both aluminum and carbon/epoxy composite plates. Wave mode velocities calculated from the measured arrival times were found to be in good agreement with

predictions obtained using both the Disperse code and finite element analysis. Differences in the relative strength of the received wave modes, the overall signal strengths and signal-to-noise ratios were observed in both active testing as well as passive steel-ball drop testing. Finally, four sensor types were recommended for further study with instrumented low-velocity impact experiments.

2.2 Introduction

The use of composites in the aerospace industry continues to increase, owing to their light weight and high strength-to-weight and stiffness-to-weight ratios as well as their applicability for economical manufacturing of complex structures. However, composites are also prone to various damage modes when subjected to low-velocity impacts or transportation loading conditions. Failure modes such as delaminations, fiber breakage and matrix cracking are likely to occur in such impact events (Diamanti & Soutis, 2010). Therefore, impact damage detection and location estimation remain a prime concern in many structural applications. Structural Health Monitoring (SHM) allows for constant monitoring for possible damage inducing events and the possibility of estimating the type of damage produced in a composite structure (Prosser et. al., 1999). In some cases, SHM systems may allow the design of composite structures to damage tolerance levels based on barely detectable rather than barely visible damage criteria. Such a change is expected to permit a significant mitigation of excess conservatism and substantial reductions of material and manufacturing costs. Additionally, maintenance cost may also be significantly reduced since inspection of the structure may be reduced to regions or parts identified by the SHM system.

Acoustic Emission (AE) based SHMs typically require the use of sensor networks that are affixed to the surface of the structure to allow real-time acquisition of AE signals from impact events. The characteristics of these received signals can be used to detect an impact event, estimate the impact location, and possibly determine the formation and type of damage produced from the impact. The reliability of a structure equipped with such a SHM system is therefore improved for real-time applications (Prosser et. al., 1999). Currently, the use of SHM is of great interest for impact location estimation as well as damage detection in a variety of applications.

With a variety of available AE sensors exhibiting different characteristics and responses to varying impact events, comparative performance evaluations are useful for identifying their suitability for use in AE-based SHM systems. When a structure is excited upon external impact, the transmission of the AE signal from the structure to the bonded sensors and the characteristics of the received waveform are dependent on the sensor properties. Based on these response attributes, the sensor response information on wave mode Time Of Arrival (TOA) and velocity estimation can be used for impact location identification. Therefore, sensor selection is an important consideration in the development of an SHM system. Since a wide range of wave frequencies below 1 MHz are expected to be generated from a spectrum of possible impacts, a broadband sensor response is a primary interest. In addition to the location estimation and damage classification, it is also imperative that the accuracy of the location estimation process be improved while decreasing the sensor footprint on the composite structure.

The impact location estimation algorithm currently under development at the University of Utah employs information based on the first wave mode arrival time at sensor

locations, and thus accurate TOA measurements are desired (Zhou & Mathews, 2014). Additionally, for an AE system to detect actual damage responses, it is important to be able to characterize a damage-inducing impact response against a representative waveform of external elements such as the source effects, wave propagation effects and/or instrument response in addition to the structural response (McLaskey & Glaser, 2012). Understanding the plate wave modes thus becomes easier with proper sensor assessment and evaluation.

2.3 AE Sensors Investigated

Based on initial research, a variety of piezoelectric sensors offering a range of characteristics were identified. Upon further discussions with industry professionals and a preliminary evaluation, six different AE sensors were selected for initial evaluation based on their performance characteristics, operating frequency range, size and ease of use, signal quality and sensitivity to realistic damage events. As shown in Figure 2.1, both permanently mounted as well as moveable sensors were considered for the sensor characterization and feasibility assessment. Each sensor is described briefly below.

Acellent's Single Smart Layer sensors are a permanently mounted and compact sensor type that uses a piezoelectric ceramic element. The overall sensor dimensions are 40 mm x 10 mm, and feature a 6 mm diameter sensor element. A polyamide high dielectric film is used to protect the element from the environment as well as noise interferences. The sensor has a weight of 1 gram and reported frequency range of 1 Hz- 5 kHz (Acellent, 2014).

Vallen Systeme's 900-RIC sensors are moveable sensors that consists of an integral 34 dB gain preamplifier and calibration bypass. The dimensions of the sensor stainless steel

casing are 29 mm in diameter x 32 mm tall, and the enclosed piezoelectric ceramic sensor element is 12.5 mm in diameter. The sensor has a reported frequency response of 100 – 900 kHz and weighs 67 grams (Vallen Systeme, 2012).

Vallen Systeme's 900-M sensors are also moveable sensors with a reported frequency response of 100 – 900 kHz. The dimensions of the sensor casing are 20 mm in diameter x 14 mm in height, have an enclosed 12.5 mm diameter sensor element and weigh 21 grams. In contrast to the 900-RIC sensor, these sensors require the use of an external preamplifier with a 34 dB gain and a 28 VDC power supply (Vallen Systeme, 2012).

Digital Wave's B1025-T sensors are another type of moveable sensor with a reported frequency response of 1 kHz – 1.5 MHz. The 9 mm diameter x 14 mm tall casing encloses a 6.3 mm diameter piezoelectric ceramic sensor element with a total weight of 8 grams. These sensors also require the use of an external preamplifier with a 20 dB gain (Digital Wave, 2014).

Steiner & Martin, Inc's Wire Lead Sensor has a piezoelectric ceramic plate that uses a SM412 piezo material. These sensors are permanently mounted and have a resonant frequency of 240 ±5 kHz. The dimensions of the sensor are 7 mm x 8 mm x 0.2 mm and they weigh less than a gram (Steiner & Martins, 2014).

SteveCo's KRNBB-PC Point Contact sensors are moveable sensors with a reported frequency response of 20 kHz – 1 MHz. The dimensions of the sensor casing are 14 mm in diameter and 28 mm in height and weighs 17 grams. The sensor encloses a nickel faceplate within a stainless steel body. These sensors require the use of a KRNWB-PC single or KRN AMP-xBB-J multichannel preamplifier (KRN Services, 2014).

2.4 Sensor Assessment and Characterization

The six piezoelectric sensors investigated were characterized based on the received signal quality and their TOA response to both active and passive testing. These test types were performed using both aluminum and carbon/epoxy composite plates. The arrival time of the initial symmetric extension (S_o) and asymmetric flexural (A_o) plate wave modes were estimated and used to calculate the mode velocities, based on the signals received by the different AE sensors under investigation.

Additionally, the signal quality and strength, as characterized by the waveform dispersion and Signal-to-Noise Ratio (SNR) were investigated and compared for the six sensor types. The frequency response of each sensor was evaluated for the two types of tests to assess sensor sensitivity. Finally, the experimental results were compared with predictions obtained using both the Disperse code and finite element analysis software, ANSYS. Disperse is commercially available software used to generate dispersion curves for multi-layered structures (Lowe, 2013) whereas ANSYS is a commercially available multi-physics finite element code (ANSYS, 2013).

2.4.1 Active and Passive Testing

Two types of tests were performed to investigate the characteristics of the six piezoelectric AE sensors: active testing and passive testing. For active testing, an AE transducer is used to produce an input signal to excite the structure. The piezoelectric sensors under investigation are used as receiving sensors to record a signal response. In the case of SHM applications, active testing would focus on changes in received sensor signals from neighboring “sending” sensors to indicate the presence of damage produced in the

structure (Grosse & Ohtsu, 2008). For passive testing, an external impact event, ranging from a pencil lead break or steel-ball drop to an actual low-velocity impact experiment, is used to provide the input signal and the AE sensors under investigation record a signal response (Grosse & Ohtsu, 2008).

2.4.2 Wave Modes and Time of Arrival Estimation

For thin plates, two primary modes of Lamb wave propagation are produced from both passive and active excitation: extensional, or Symmetric (S) modes and flexural or Asymmetric (A) modes. While each wave mode consists of in-plane and out-of-plane displacement components, the extensional (S) mode consists primarily of in-plane displacements versus out-of-plane displacements for the flexural (A) mode. Whereas the extensional mode is characterized by high-frequency components, high velocity and low to minimal dispersive nature, the flexural mode exhibits lower frequency components, lower velocity and is highly dispersive. Furthermore, A modes can travel longer distances than the S modes, making them better suited for impact location estimation in large composite structures. However the wave propagation dispersion makes the process difficult (Prosser, 1991). For impact location estimation algorithms that utilize the initial time of arrival of a received signal, only the initial S_o and A_o modes are of interest. As a result the S_o and A_o modes are the primary focus in this study.

Based on the waveform signal recorded by the candidate sensors, the time of arrival measurements for the S_o and A_o modes are recorded for each sensor type. At different locations from the impact position, d_1 and d_2, the time difference of arrival of the wave

modes, $t_2 - t_1$, is used to estimate the S_o and A_o wave mode velocities in both aluminum and carbon/epoxy composite plates using the expression

$$velocity = \frac{d_2 - d_1}{t_2 - t_1}. \quad (1)$$

For a particular sensor type, Figure 2.2 shows the waveform response recorded at two receiving locations, namely Signal A and Signal B. Red dotted lines *d1* and *d2* denote the initial time of arrival of S_o modes at these two receiving locations. The time of arrival estimates at these locations are then used to estimate the S_o mode wave velocity. The process was then repeated for the A_o wave modes.

2.4.3 Waveform Dispersion

While the extensional and flexural wave modes are the most prominent in thin plates, the number of these waves depends on the *d/l* ratio, where *d* is the thickness of the plate and *l* is the acoustic wave length. For a particular acoustic frequency, there exists a number of wave propagation modes produced in the plate with a specific wave number or a phase velocity. The presence of these multiple wave modes as well the dispersive nature of the wave mode propagation are dictated by the dispersion curves (Prosser, 1991).

Figure 2.3 shows the dispersion curve for an aluminum plate with a thickness of 1.6 mm as estimated using the Disperse software. Note that only the initial S_o and A_o modes are observed for frequency ranges lower than 1 MHz. While S_o wave mode depicts a general flat response of phase velocity over a range of the product of the frequency and thickness before it starts to descend, A_o mode shows a continuous ascending curve for every increment therefore causing higher phase velocity dispersion. Above 1 MHz, higher

order Lamb waves, S_1 and A_1, extending to further S_n and A_n modes are also observed that make mode separation extremely difficult. For this sensor assessment, therefore, only lower frequencies below 1 MHz are used, both for active and passive (steel-ball drop) testing. In doing so, only S_o and A_o wave modes are expected to eliminate any possible convolution of higher frequency modes.

2.4.4 Signal-to-Noise Ratio

In signal processing, a Signal-to-Noise Ratio (SNR) quantifies the noise power corrupting the received signal power. A ratio higher than 1:1 means higher signal power than noise power and is desired for all sensor types. For an ideal signal with no noise and a zero-mean, the SNR is the ratio of squares of the signal variance to the noise variance (Ponnala, 2007), or

$$SNR = \frac{\sigma_{signal}^2}{\sigma_{noise}^2}. \quad (2)$$

For actual sensor signals, the signal power includes some level of noise. For a sufficiently large sample size, the noise can be considered non zero and statistically independent of the signal (Ponnala, 2007). In addition, the mean noise should be removed from the received signal to avoid the DC bias. The Signal-to-Noise Ratio in such a case can be written as:

$$SNR = \frac{\sigma_{signal}^2}{\sigma_{noise}^2} - 1. \quad (3)$$

The SNR in the decibel scale can then be written as

$$SNR_{dB} = 20log_{10}(SNR). \quad (4)$$

2.5 Experimental Setup

Sensor evaluations were performed using two 1.2 m square test panels. The first panel, a 1.6 mm thick 6061-T6 aluminum plate, was used for active and steel ball drop testing. Aluminum is isotropic in nature and has stiffness properties that are approximately constant in all directions, therefore making preliminary comparison easier for sensor evaluation. The second panel was a 16-ply (2.3 mm) thick quasi-isotropic $[0_2/45_2/90_2/\text{-}45_2]_s$ composite plate that was fabricated from Hexcel IM7/8551 carbon/epoxy unidirectional prepeg.

A National Instruments (NI) PXIe-1073 data acquisition system coupled with NI LABVIEW and MATLAB scripts were used for data collection and signal processing. For the Acellent single smart layer, Vallen Systeme 900-M, Digital Wave B1025T, KRNBB-PC and STEMiNC Wire Lead sensors were used with an AMP-4BB-J external preamplifier with 27 dB gain and internal 28 VDC power supply to boost the output signal strength. The Vallen Systeme's 900-RIC sensor required a decoupling circuit to remove the AC component from the signal prior to data acquisition.

To reduce impedance mismatch between the test panel and the sensor for better signal transmission, Vishay M-Bond 200 adhesive and Sonotech's High Z-HV couplant were used for the permanently mounted and moveable sensors, respectively. For proper mounting and consistency purposes, polyethylene templates were used for sensor placement at the desired locations. These templates were drilled and threaded at specific

locations to custom fit each moveable sensor type to ensure proper bonding onto the test panel and prevent sensor movement.

2.5.1 Frequency Response Evaluation

A frequency response evaluation was performed for all six sensor types to determine their working frequency range on both aluminum and composite test panels. Since a wide range of AE monitoring is performed at frequency levels below 1 MHz, an input frequency range of 50 to 500 kHz with 50 kHz increments was used. The Acellent Single Smart Layer was used as a transducer for all active testing experiments owing to its broadband frequency range, low profile and permanent bondage to the test panel. Therefore the input signal and phase change were assumed constant for all sensors. A 5-cycle sinusoidal input signal was applied to the center of the test panel and the receiving sensor was placed 178 mm from the transducer. At each frequency, active testing was performed 10 times for each sensor to compute the sensor response for S_o and A_o plate wave modes.

For preliminary analysis of velocity estimation, the Disperse code was used to approximate particular wave modes' phase velocities at different frequencies using their specific material properties. Figure 2.4 shows the dispersion curve of S_o and A_o wave mode velocities at different input frequencies for an aluminum plate. These estimates were used to separate the plate wave modes for further verification with sensor response analysis.

2.5.1.1. Sensor Response Estimation

The output response of a Linear Time-Invariant (LTI) system, *Y(f),* can be characterized in the frequency domain using the convolution theorem such that

$$Y(f) = X(f) \cdot H(f), \tag{5}$$

where *X(f)* is the input signal (impulse) and *H(f*) is the system response to an impulse (Proakis & Maolakis, 2007). The system response consists of multiple components including instrumentation, coupling, structural and sensor properties. Assuming the system response is only affected by the plate response, $H_p(f)$, the actuator response, $H_a(f,)$ and the receiving sensor response, $H_r(f)$, further analysis was performed to assess the sensor performance on the current setup.

$$H(f) = H_p(f) \cdot H_a(f) \cdot H_r(f), \tag{6}$$

Furthermore, for a single actuator type, the input signal response was estimated and separated along with the plate response from the output signal response of the plate wave modes S_o and A_o therefore estimating the receiving sensor frequency response. An approximated time interval was chosen for both S_o and A_o mode propagation based on Disperse velocity simulation. For a particular wave number *k(f)* and an actuating distance *r*, the ratio of the input frequency *f* and the phase velocity V_{ph} is different for both S_o and A_o mode waveforms. Therefore, the magnitude of the plate response $H_p(f)$ can be estimated using the Fast Fourier Transform (FFT) of the input and received signal response as (Harley & Moara, 2013)

$$\left|H_p(f)\right| = \frac{|Y(f)|}{|X(f)|\sum_m \sqrt{\frac{1}{k(f)r}}} = \frac{|Y(f)|}{|X(f)|\sum_m \sqrt{\frac{V_{ph}}{rf}}} = \left|\frac{Y(f)}{X(f)}\right| \sqrt{\frac{rf}{V_{ph}}}. \tag{7}$$

Figures 2.5 (a) and (b) show the frequency response analysis of S_o and A_o modes, respectively, for each sensor type. Vallen Systeme's 900-RIC showed the strongest overall

signal response for S_o while KRNBB-PC showed a stronger response for the A_o wave mode, particularly at the midrange of frequencies investigated. It is to be noted that these results are used to understand the strength of the received waveforms at particular input frequencies and are valid for the said setup only. Some discrepancies between the S_o and A_o mode frequency responses were observed as a result of wave mode propagations and approximated time intervals using the predicted values of Disperse simulations. Nevertheless, based on the signal strengths at the approximated sensor bandwidth, 300 kHz was chosen as the best-suited input frequency for all six AE sensor types. Thus this frequency was selected for active testing in further sensor evaluations.

2.5.2 Active and Passive Testing

For active testing, the input signal was introduced at the center of the test panel. The response signal was recorded by two receiving sensors from each sensor type that were placed at two different distances from the input signal: 178 mm and 228 mm. These distances were selected to effectively separate the S_o and A_o wave modes at the sensor locations and to avoid reflections from the edges of the 1.2 m square plate. As chosen from the frequency response analysis, a 5-cycle input signal was applied at a 300 kHz excitation frequency and a 2 MHz sampling frequency range to excite the structure. Testing was performed 20 times for each sensor type and the averaged data from each location were used for further signal analysis and TOA estimation.

For passive testing, a 12.7 mm diameter steel ball was dropped from a 152 mm height through a steering tube to a point at the center of the test panel. AE sensors were placed at the same two distances (178 mm and 228 mm) as used for active testing to record

the impact response. The drop experiments were repeated 10 times for consistency of signal quality investigation.

2.5.3 Disperse Simulation

For this comparative evaluation study, dispersion curves for both aluminum and composite plates were calculated as per the material properties. Aluminum has a material density of 2.7 gm/cm^3 and the elastic properties are frequency and direction independent. For the composite plate, the plies are modeled using material properties in their local material coordinate system. The density of the IM7/8551 carbon/epoxy composite material used is 1.57 gm/cm^3 and each ply is 0.14 mm thick. Table 2.1 lists the elastic properties of the IM7/8551 composite material.

2.5.4 Finite Element Analysis

To assist the evaluation of the recorded sensor responses during active testing, wave propagation of the 5-cycle tone burst input signal at 300 kHz frequency was simulated using finite element analysis. The commercial finite element code ANSYS was used to perform the three-dimensional dynamic analyses. Eight-node brick-type elements were used and displacement boundary conditions were applied to produce the input signal and the far-field support constraint as shown in Figure 2.7 (a). A representative three-dimensional "strip" of the test panels (400 mm in length x 5 mm in width x 2.3 mm in thickness) was used to reduce computational time. Response waveforms were recorded at the same two distances from the excitation input location used in testing: 178 mm and 228 mm. Two separate analyses with either in-plane or out-of-plane displacement signal inputs

were used to investigate the S_o and A_o wave modes, respectively, as shown in Figure 2.6 (b). A 0.0625 μsec time step corresponding to a 16 MHz frequency response was used in the model and damping was not considered (Kim et. al., 2014).

2.6 Results

For active testing, averaged raw signals were used for sensor evaluation and TOA determination to avoid loss of any response data. The received output signals were compared with finite element simulation results for both TOA and velocity estimates. The finite element analyses did not incorporate a damping factor, and therefore did not produce the attenuation that exists in the actual test conditions. In this investigation, however, results from finite element simulations are used only for velocity comparison as well as S_o and A_o wave packet correlations.

2.6.1 Velocity Estimation Using Simulation Softwares

An input frequency of 300 kHz was used in the Disperse code and wave velocities for both symmetric (S_o) and asymmetric (A_o) modes were extracted from the dispersion curves. Similarly, finite element analyses were used to calculate the wave mode velocities using the time difference of arrival between two locations (178 mm and 228 mm). Figure 2.8 shows the S_o and A_o wave mode for active testing at a receiving location of 178 mm Separation of these plate wave modes is significant for accurate time of arrival estimation.

Table 2.2 lists the predicted wave mode velocities for both the aluminum and composite plate using the Disperse code and ANSYS finite element analysis at an input frequency of 300 kHz. Using the time difference of arrival estimation, as discussed in

earlier section, the wave mode velocities were estimated. The simulated and theoretically predicted wave mode velocities using both analysis methods were found to be in good agreement.

2.6.2 Waveform Evaluation and Velocity Estimation for Active Testing

For an input frequency of 300 kHz, both symmetric (S_o) and asymmetric (A_o) wave components were visible in the received signals from all six sensors types. For a 5-cycle input frequency, both S_o mode and A_o mode showed minimal to low dispersive nature of received wave packets for the aluminum test panel. As shown in Figure 2.9, a good signal amplitude response was observed for all sensor types. VS 900-RIC showed the largest S_o amplitude response (0.38 V) and DW B1025T showed the lowest at 0.006 V. The KRNBB-PC sensor showed the strongest response of the A_o wave packet at 2.8 V and the DW B1025T showed the lowest response of 0.006 V. Comparing the amplitude of the received S_o and A_o modes, the KRNBB-PC sensors showed the larger amplitude difference (0.28 V for S_o to 2.8 V for A_o) whereas the DW B1025T showed similar amplitudes for both wave modes. Additionally, random noise components between the wave packets were observed to be lower for the Acellent SSL, STEMiNC Wire Lead and KRNBB-PC sensors.

An excitation signal causes multiple wave modes, which propagate at different velocities. With increasing distance from the input signal, the total wave energy spreads, therefore causing dispersion [2]. Such dispersion is higher in the case of the composite plate as shown in Appendix D. A higher attenuation of the A_o wave packet and higher noise signal component were seen for all the sensor types for the composite plate. This result was believed to be due to the multiaxial laminated nature of the composite plate. As a result of

multiple layers with different fiber orientations through the panel thickness, additional reflections from each layer interface are believed to occur in the composite panel. Additionally, random noise resulting from instrument setup, cable interference, and BNC cable connections adds to these responses.

At a 300 kHz input frequency, both high-frequencies S_o and low-frequency A_o mode components were observed in all cases, but with some dispersive modes of lower amplitudes in between. This dispersive nature is believed to be a combined effect of the structural response in addition to instrument response, sensor type and the coupling mechanism. For a 5-cycle input signal, Acellent SSL sensor showed a good amplitude response owing to its permanent bondage to the structure. However, some additional wave components were observed in the S_o wave mode. The STEMiNC sensor showed comparable response to the Acellent SSL sensor, but with a slower A_o mode arrival time. The Vallen Systeme 900-M sensor also displayed significant noise components in comparison with the received wave modes. It is noted that the sensor element in the Vallen Systeme and Digital Wave moveable sensors is enclosed in a stainless-steel casing, which may reduce electromagnetic noise interference. However, additional "ringing" was observed with these sensors, which adds to the noise dispersion and makes initial arrival time estimation more difficult, especially for the A_o mode. The KRNBB-PC sensors showed a higher amplitude response for the A_o wave mode. In addition, lower received signal amplitudes were recorded in comparison to the ±5 Volt input excitation signal in active testing. This was believed to be due to the response signal from an impact point attenuating over a longer distance in the test specimen.

Based on the experimental signal responses, the time difference of arrival was estimated at five different locations on the response signal to account for the discrepancy caused due to dispersion. This assessment method was performed on all sensor types for consistency purposes. As a result, the initial time difference of arrival estimation for the S_o mode was slower than the average estimated time difference. Figure 2.10 shows the standard deviation error bar (1σ) for the time difference of arrival on the aluminum plate. The relative difference was found to be comparable for all sensor types. A similar observation is seen for the composite plate as well (See Appendix E).

Based on the average time difference of arrival of all the sensor types, the S_o and A_o mode velocities were calculated. Table 2.3 shows the comparison between predicted wave mode velocities and those determined experimentally for both the carbon/epoxy composite and aluminum panels using the six AE sensors investigated. The measured wave velocities are in good agreement with the predictions from both the Disperse and ANSYS analyses.

In conjunction with the dispersion curve of aluminum, the S_o arrival time was relatively independent of input frequency and minimal dispersion was observed. In contrast, the A_o mode exhibited wave property dependence particularly on input frequency. Preliminary study also suggested wave mode velocity dependence on material thickness. A better correlation with the Disperse and ANSYS results is found for the flexural A_o mode due to the approximated time intervals. While the permanently mounted Acellent single smart layer sensor showed good agreement with predictions for both wave mode components in aluminum, the moveable Digital Wave's B1025-T sensor showed better agreement for the composite plate.

2.6.3 Waveform Evaluation for Steel Ball Drop Testing

For steel-ball drop testing, raw signals were used for wave mode detection and signal evaluation to avoid loss of imperative data. Such passive experiments are representative of low-velocity impacts that are of interest in real time SHM, where the impact type and source are unknown and signal filtering range is unpredictable. Experimental results showed that the steel ball drop testing produced both S_o and A_o wave modes, but the flexural A_o mode was predominant due to the stronger out-of-plane input condition (See Figure 2.11). The S_o wave mode amplitudes were comparable to those from the random noise signals making arrival time estimations difficult. While the nature of the signals remained similar, the Digital Wave B1025-T sensor exhibited a lower SNR of 9.58 dB and Acellent SSL showed the highest SNR of 39.62 dB.

As shown in Figure 2.11 (b), for the VS 900-RIC sensor that has an inbuilt preamplifier, the high-frequency S_o mode component was visible but of much lower amplitude and required higher magnification than the A_o wave mode. Similar to observations from active testing, the composite plate showed smaller wave packet amplitudes as compared to aluminum.

For a passive testing condition such as a steel ball drop, the input signal produces multiple frequency responses with both high and low frequency components. As shown in Figure 2.10, the low-frequency A_o acoustic responses were dominant for all sensor types. The Acellent SSL, Vallen Systeme, Digital Wave and STEMiNC sensors showed a broadband wave packet response. The integrated preamplifier and calibration bypass used in Vallen Systeme's 900-RIC produced noise signal suppression and wave mode amplification within its effective operable range. The external preamplifier produced signal

amplification for the other four sensors. However, signal filtering was not applied, and thus a broad spectrum response of both low frequency and high frequency components was observed in these cases. For the KRNBB-PC sensors, which are classified as *displacement* sensors, a significant signal response was recorded upon impact with greater amplitude than the subsequent acoustic responses. This initial response, believed to be the associated with the surface displacement upon impact, results from the sensor sensitivity to extremely low-frequency components. However, this additional response obtained during the steel ball drop impact testing produced a more complex overall sensor signal in comparison to the other sensors, which are primarily classified as *velocity* sensors and are less sensitive to surface displacements.

For the aluminum panel, the S_o mode was of much smaller amplitude but somewhat distinguishable as shown in Appendix F. In all cases, lower amplitude of higher frequency components and higher amplitude of lower frequency components were observed. Likewise, the Acellent SSL sensor showed a higher signal magnitude and the DW B1025T sensor showed the lowest SNR.

The SNR response of each sensor type with a 1σ error bar is calculated for all sensor types at both receiving locations of 178 mm and 228 mm. Figure 2.12 shows the SNR for steel ball drop testing using the composite plate. A similar response for the aluminum plate is shown in Appendix G. As expected, a considerable drop in the SNR is observed over an increased propagating distance. A comparable difference in SNR is observed for all sensor types between the two distances. The Acellent SSL, Vallen Systeme, STEMiNC and KRNBB-PC sensors exhibited higher SNRs and carried higher energy signals. The VS 900-M, DW B1025T and STEMiNC showed minimal error bar deviation in SNR

estimation. Similar responses were observed in the case of the aluminum panel (See Appendix H). A minimal SNR drop was observed for Acellent SSL, DW B1025T, STEMiNC and KRNBB-PC sensors for the isotropic aluminum panel.

For low frequency input conditions on thin plate structures, the S_o modes show minimal velocity changes and therefore are considered less dispersive in nature. However, for lower frequency inputs, the modes attenuate much faster therefore making it difficult for time of arrival estimation in larger structures. In such cases, the A_o mode may be of greater use for structural health monitoring of larger areas.

2.7 Summary and Conclusions

A comparative evaluation of six commercially-available piezoelectric AE sensors was performed to assess their performance in plate wave mode detection and received signal quality using both aluminum and composite panels. The sensors that exhibited higher signal strength and lower wave packet dispersion were preferred for wave mode assessment and time of arrival estimation. Active testing was performed using a transducer to produce an input signal to excite the structure while the receiving AE sensors recorded a response. Arrival times of both the S_o and A_o plate wave modes were determined for each sensor type. Wave mode velocities calculated from the measured arrival times were found to be in good agreement with predictions obtained using both the Disperse code and finite element analysis simulation. In general, the wave modes received in the laminated carbon/epoxy composite panel were more dispersive than in the aluminum panel. Differences in the relative strength of the received S_o and A_o wave modes as well as the overall signal strength and noise levels were observed between the six sensor types.

Additionally, steel-ball drop tests were performed using each sensor type to record the impact response. While both S_o and A_o wave modes were produced, the flexural A_o mode was dominant in the recorded signal response for all sensors investigated. Similar to active testing, lower signal amplitudes of wave modes were observed in the composite panel in comparison to the aluminum panel. Significant differences were observed in the received signal responses for the six sensor types, including the received signal strength and the signal-to-noise ratio.

While completely understanding the behavior of the plate modes remain an issue, good correlation of TOA with Disperse and FE model outputs was observed. It was also observed that the signal strength and quality were highly affected by the material properties and instrument responses in addition to the structure response itself. For the current impact location estimation algorithm in progress at University of Utah, accurate initial time of arrival estimation is vital for the impact location assessment and damage evaluation. While a majority of the damages for low-velocity impacts lead to delamination that carry lower frequency components, subsurface damages such as fiber breakage carry higher frequency components and must be identified for source localization. In such a case, sensors that permit accurate amplitude outputs to such event for accurate TOA estimation were desired. Additionally, comparable responses to both low-frequency and high-frequency wave mode components are desired to confidently characterize damage types. While all the sensor types showed comparable results for active testing, the Acellent SSL, VS 900-M, DW B1025T and STEMiNC Wire Lead sensors showed good frequency response results based on signal quality, TOA extraction and comparable SNR deviation over a propagating distance for passive testing conditions.

For in-situ applications, ease of sensor attachment and data acquisition was desired. Acellent's single smart layer and STEMiNC sensors are low profile and easy to bond to the outside of composite structures. However, the moveable Vallen Systeme and Digital Wave's sensors can be moved around as desired for impact location estimation. Additionally, Digital Wave's B1025-T and KRNBB-PC sensors have smaller diameter and are threaded on both ends therefore providing a secure bondage to the test structure. While preamplifiers were convenient for preliminary testing, use of multiple cables and extended transmission time to the data acquisition system may lead to the loss of imperative data. Moreover, reduced impedance mismatch was desired between the source of impact and sensing element for better signal response. Acellent, Vallen 900-M, Digital Wave and STEMiNC sensors have a smaller sensor element providing higher confidence for their depicted wave mode sensitivity and signal quality. Also, it was observed that the sensor element highly affected the mode dominance in these particular tests, with extensional mode prominent in active testing and flexural mode in out-of-plane impact testing.

Based on the testing of all six sensor types, four sensor types, Acellent SSL, Vallen Systeme's 900-M, Digital Wave's B1025T and STEMiNC's Wire Lead sensors showed the most promising results and were thus recommended for future studies with instrumented low-velocity impact conditions. Future comparative evaluation on candidate AE sensors will focus on assessing sensor performance for use in impact location estimation algorithms as well as detecting and classifying damage produced in composite structures due to impact events.

2.8 Acknowledgment

This work is supported in part by the National Aeronautics and Space Administration (Award No. NNM13AA12G) and the Air Force Office of Scientific Research (Award No. FA95501210291).

2.9 References

Acellent Technologies, Inc. (n.d.). Standard smart layer. Retrieved from http://www.acellent.com/blog1/products/sensors/standard-smart-layer/

ANSYS Inc. (2013). ANSYS Help manual version 15.0.

Diamanti, K., & Soutis, C. (2010). Structural health monitoring techniques for aircraft composite structures. *Progress in Aerospace Sciences*, *46*(8), 342-352.

Digital Wave. (n.d.). B1025T- Broadband acoustic emission sensor. Retrieved from http://digitalwavecorp.com/MAE-051414-%20B1025T%20Sensor.pdf

Grosse, C. U., & Ohtsu, M. (2008). Introduction. In *Acoustic emission testing: [basics for research, applications in civil engineering]* (pp. 3-6). Berlin: Springer.

Harley, J. B., & Moura, J. M. (2013). Sparse recovery of the multimodal and dispersive characteristics of lamb waves. *Journal of the Acoustical Society of America*,*133*(5), 2732–2745.

Kim, S., Uprety, B., Mathews, V. J., & Adams, D. O. (2014). Numerical simulation and experimental validation of lamb wave propagation behavior in composite plates. *AIP Conference Proceedings, Annual Review of Progress in QNDE*, Boise, Idaho.

KRN Services. (n.d.). SteveCo KRNBB-PC point contact sensor. Retrieved from http://www.krnservices.com/documents/krnbb-pc_specs.pdf

Lowe, M. (2013). Disperse software, Imperial College London.

McLaskey, G. C., & Glaser, S. D. (2012). Acoustic emission sensor calibration for absolute source measurements. *Journal of Non Destructive Evaluation*, *31*(2), 157-168.

Ponnala, L. (2007). Free energy signal characterization. In *Analysis of Genetic*

Translation Using Signal Processing (p. 13). (Doctoral dissertation, North Carolina State University)

Proakis, J. G., & Manolakis, D. G. (2007). Frequency domain analysis of lti system. in *Digital Signal Processing* (pp. 312-314). NJ: Pearson Prentice Hall.

Prosser, W. H., Gorman, M. R., & Humes, D. H. (1999). Acoustic emission signals in thin plates produced by impact damage. *Journal of Acoustic Emission*, *17*(1-2), 29-36.

Prosser, W. H. (1991). *The propagation characteristics of the plate modes of acoustic emission waves in thin aluminum plates and thin graphite/epoxy composite plates and tubes* (Doctoral dissertation, John Hopkins University).

Steiner & Martins, Inc. (n.d.). Piezoelectric ceramic plate transducer 240 khz – Steminc. Retrieved from http://www.steminc.com/PZT/en/piezo-ceraminc-plate-7x8x02mm-wire-lead-240-khz

Vallen Systeme. (2012). Acoustic emissions sensors specification. Retrieved from http://www.vallen.de/sites/default/files/sov1212_0.pdf

Zhou, J., & Mathews, V. J. (2014). Impact location estimation in anisotropic structures. *AIP Conference Proceedings, Annual Review of Progress in QNDE*, Boise, Idaho.

Table 2.1. Elastic Properties of IM7/8551 Carbon/Epoxy.

Material Property	Value
E_{11} (Pa)	1.66E+11
E_{22} (Pa)	8.56E+09
E_{33} (Pa)	8.56E+09
G_{12}(Pa)	5.60E+09
G_{13}(Pa)	5.60E+09
G_{23}(Pa)	2.94E+09
ν_{12}	2.69 E-01
ν_{13}	2.69 E-01
ν_{23}	4.56 E-01

Table 2.2. Predicted Wave Mode Velocities.

Material Type	Wave Mode	Predicted Wave Mode Velocity (mm/μs)	
		Disperse	ANSYS
Aluminum	So	5.33	5.35
	Ao	2.89	2.92
Composite	So	5.63	5.83
	Ao	1.78	1.64

Table 2.3. Active Testing Wave Mode Velocity Predictions and Measurements.

Material Type	Wave Mode	Predicted Wave Mode Velocity (mm/μs)		Measured Wave Mode Velocity(mm/μs)					
		Disperse	ANSYS	Acellent SSL	VS 900RIC	VS 900M	DW B1025T	STEM iNC	KRN BB-PC
Aluminum	**So**	**5.33**	**5.35**	**5.29**	**5.91**	**5.64**	**5.24**	**5.47**	**5.20**
	Ao	**2.89**	**2.92**	**2.84**	**2.97**	**2.50**	**2.81**	**2.50**	**2.97**
Composite	**So**	**5.63**	**5.83**	**5.41**	**5.41**	**5.04**	**5.78**	**6.20**	**5.29**
	Ao	**1.78**	**1.64**	**1.67**	**1.65**	**1.75**	**1.65**	**1.69**	**1.52**

(a) (b) (c) (d) (e) (f)

Figure 2.1. AE Sensors Under Evaluation (a) Acellent Single Smart Layer (b) Vallen Systeme 900-RIC (c) Vallen Systeme 900-RIC (d) Digital Wave B-1025T (e) STEMiNC Wire Lead (f) SteveCo KRNBB-PC.

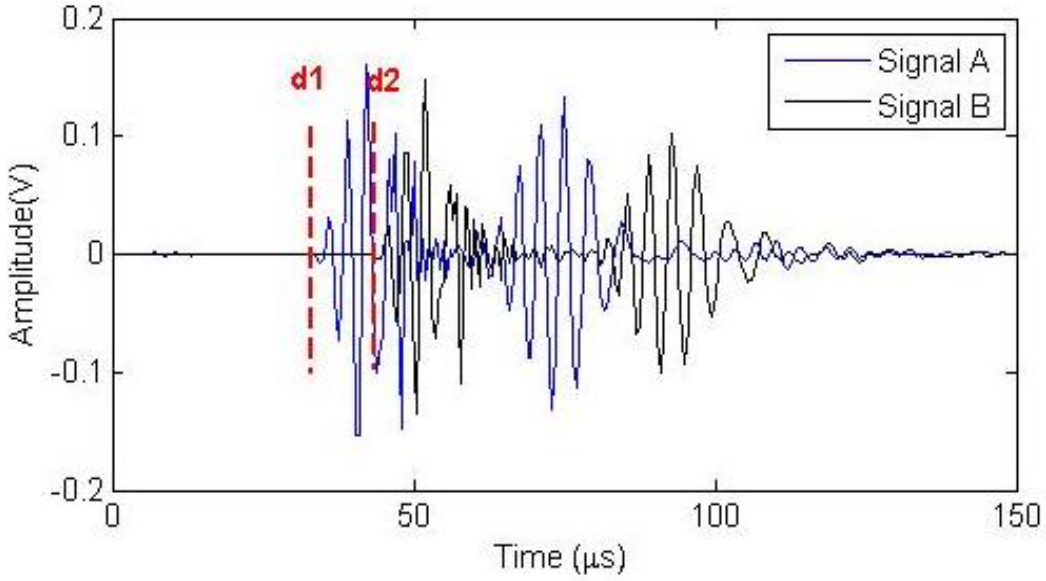

Figure 2.2. Time of Arrival Estimation.

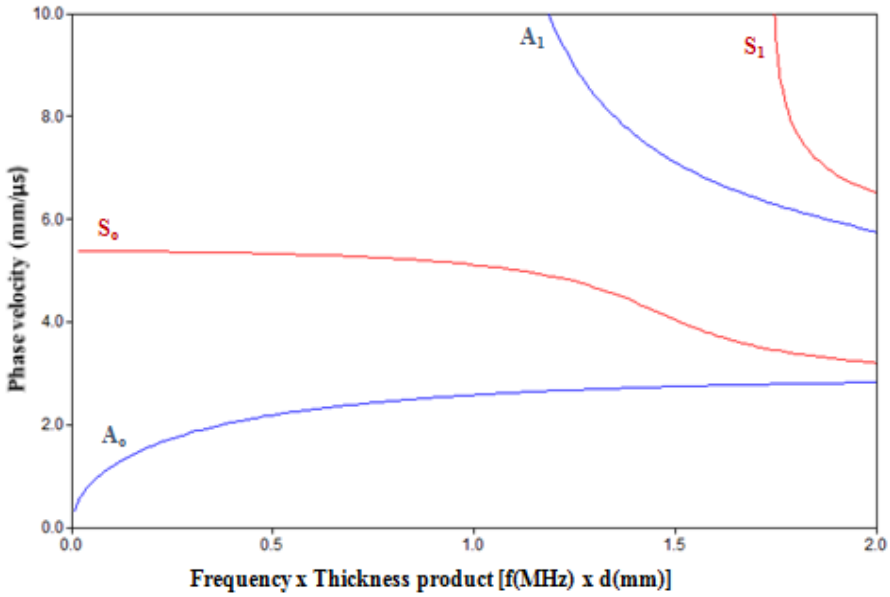

Figure 2.3. Dispersion Curve of Aluminum Plate.

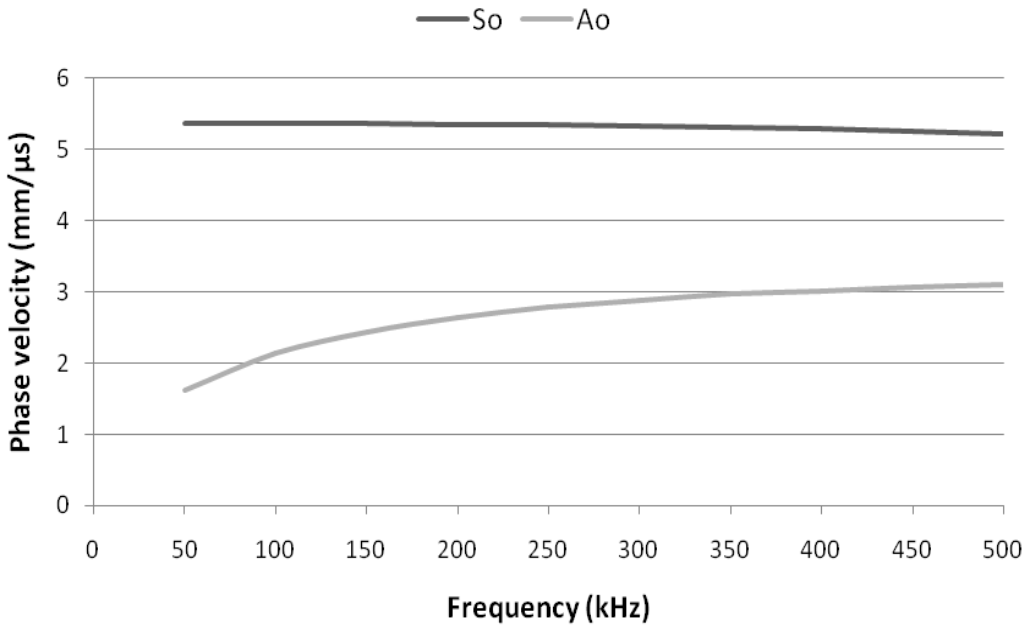

Figure 2.4. Dispersion Curve of Aluminum Plate Using Input Frequencies 50 – 500 kHz.

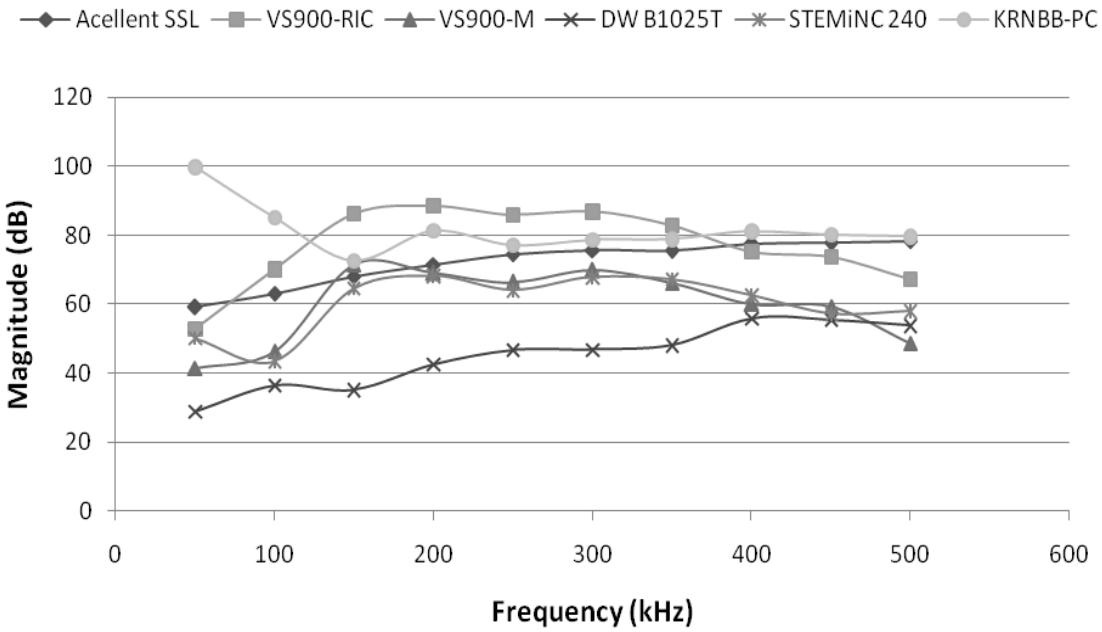

(a)

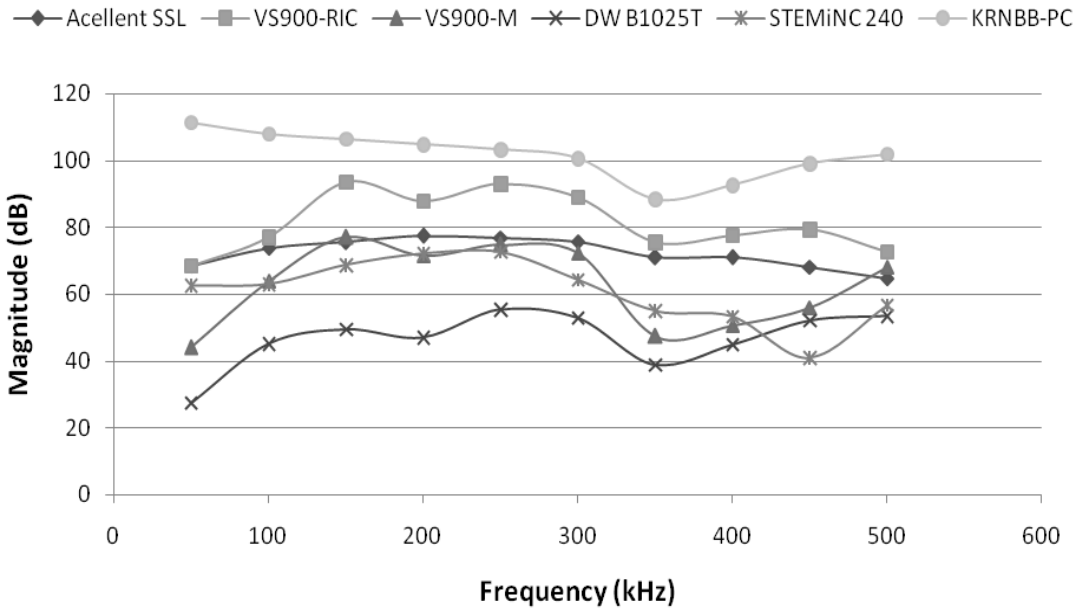

(b)

Figure 2.5. Frequency Response Analysis of All Sensor Types (a) S_o Wave Mode (b) A_o Wave Mode.

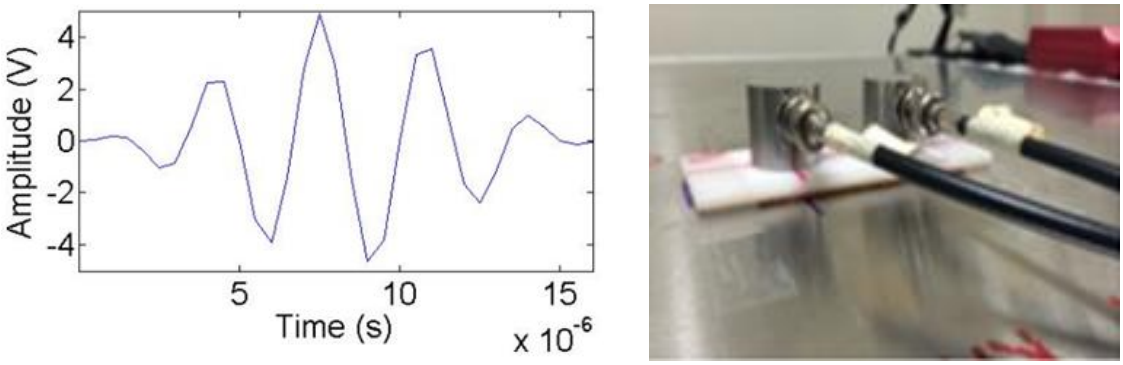

Figure 2.6. Basic Setup of Active Testing (a) Excitation Signal for Active Testing (b) Two Receiving Sensors (VS 900-RIC).

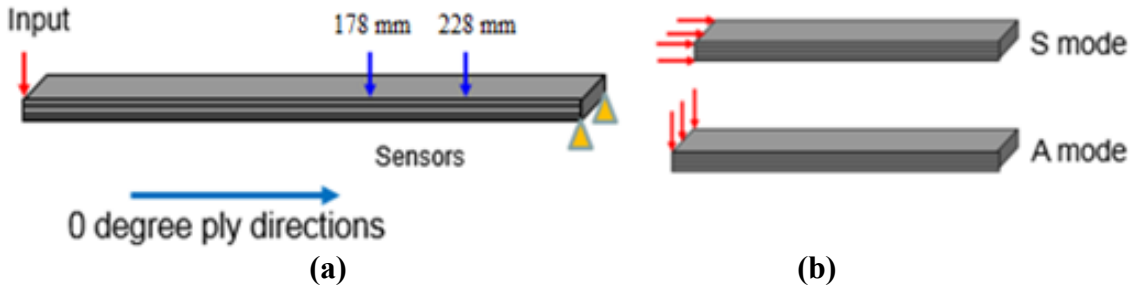

Figure 2.7. Finite Element Analysis (a) Finite Element Modeling Method Used at Two Receiving Sensor Locations (b) Two Input Type (In-Plane and Out-of-Plane) Used for Corresponding Wave Mode Estimation.

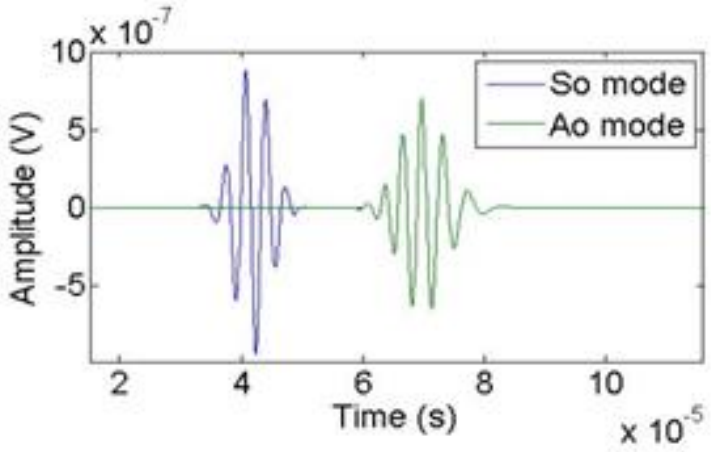

Figure 2.8. Results from Finite Element Analysis of Wave Propagation in an Aluminum Plate for a 300 kHz Input Signal Frequency.

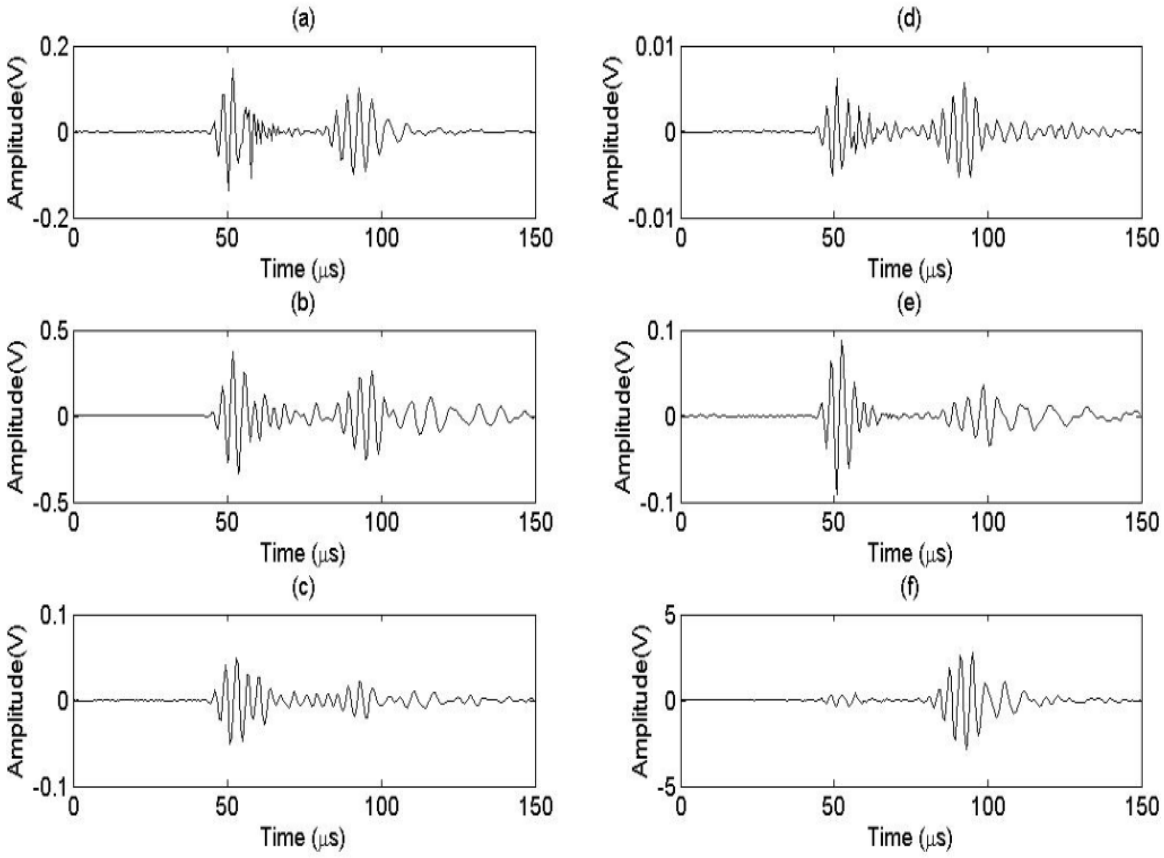

Figure 2.9. Active Testing Results on Aluminum Test Panel (a) Acellent Single Smart Layer (b) Vallen Sensor 900-RIC (c) Vallen Sensor 900-M (d) Digital Wave B1025T (e) STEMiNC Wire Lead (f) SteveCo KRNBB-PC.

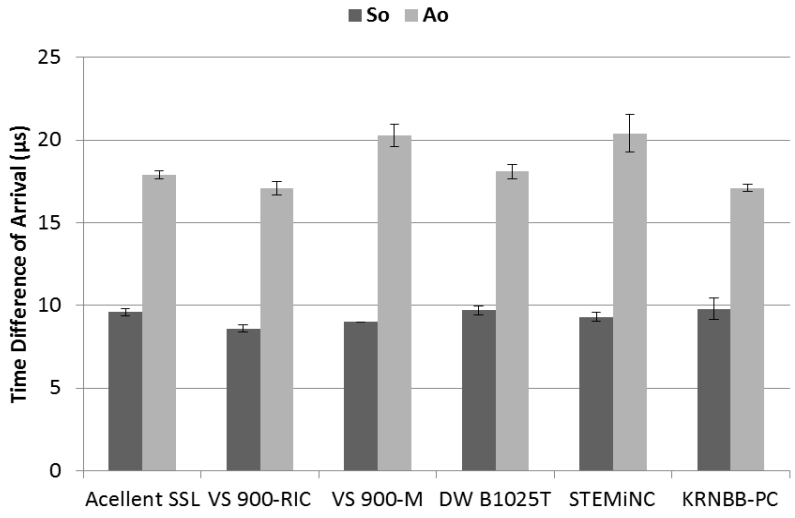

Figure 2.10. Time Difference of Arrival Estimation from Aluminum Plate.

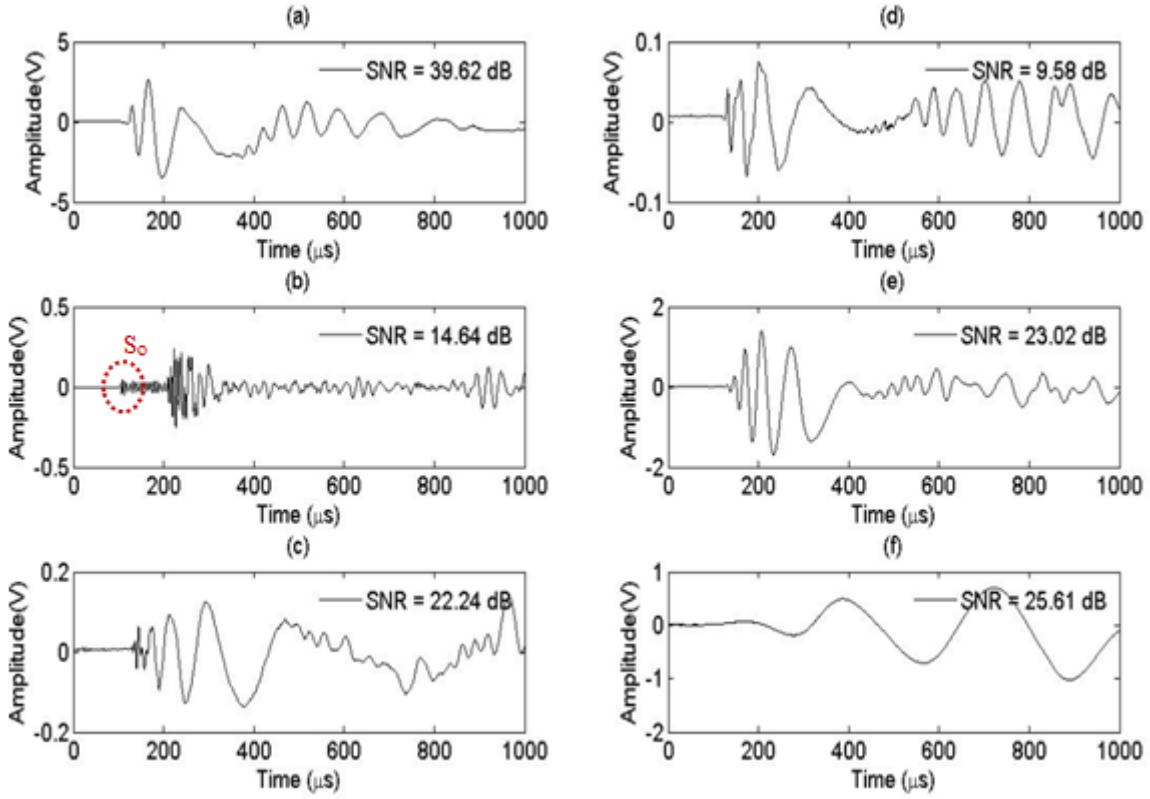

Figure 2.11. Steel Ball Drop Testing Results on Composite (a) Acellent Single Smart Layer (b) Vallen Sensor 900-RIC (c) Vallen Sensor 900-M (d) Digital Wave B1025T (e) STEMiNC Wire Lead (f) SteveCoKRNBB-PC.

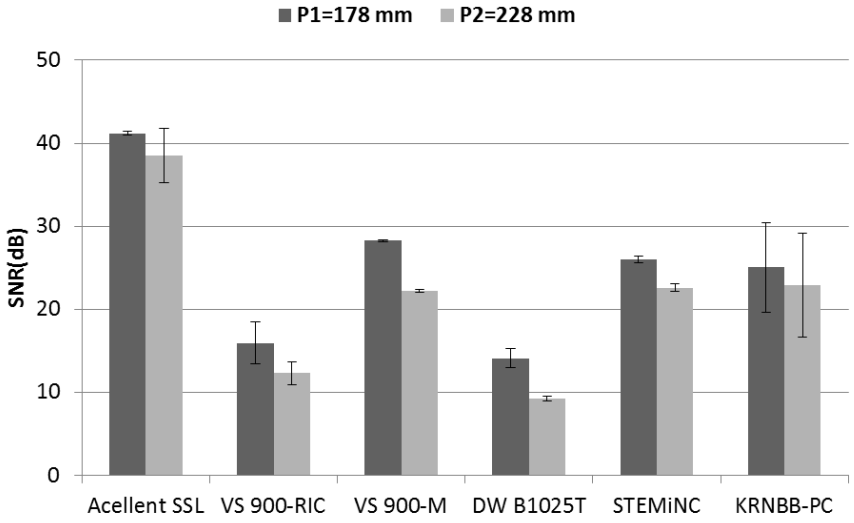

Figure 2.12. Signal-to-Noise Ratio (SNR) Estimation on Composite at Two Receiving Locations P1 and P2.

CHAPTER 3

ACOUSTIC EMISSION-BASED DAMAGE CHARACTERIZATION IN COMPOSITE PLATES USING LOW-VELOCITY IMPACT TESTING

3.1 Abstract

Low-velocity impact experiments help simulate real-time impact events on composite structures that could initiate barely visible to barely detectable damage types. In doing so, Acoustic Emission (AE) based Structural Health Monitoring (SHM) allows for the use of sensing technologies to monitor and classify such impact events and classify the damage types. The understanding of signal waveforms and damage inducing events could significantly increase reliability of aerospace structures by increasing the factor of safety. In this study, quasi-isotropic carbon/epoxy laminates were used to perform low-velocity impact testing using instrumented drop towers, and piezoelectric sensors were used for data acquisition. Both edge-clamped and back-face supported boundary conditions were used with varying instrumented tup to initiate particular damage modes such as matrix cracking, delaminations and fiber breakage. Further damage assessments were performed using ultrasonic C-scan testing and microscopic investigation. Matrix damage was the first

failure mode to initiate, characterized with low-frequency carrying components. For an edge-clamped boundary condition, damage further propagated to interply delaminations with frequency components up to 150 kHz. Back-face support condition showed combination damage modes of matrix cracking, delaminations, debonding and fiber failure with higher energy frequency carrying components up to 500 kHz. The C-scan images of the damage condition showed significant fiber breakage at the vicinity of impact area.

3.2 Introduction

Composites are a primary choice in today's aircraft and aerospace industries due to their high specific strength and stiffness, low weight and wide applicability in structural design (Diamanti & Soutis, 2010). However, unlike metal structures, composite structures are more susceptible to internal impact damage that ranges from barely visible to barely detectable. Such damage conditions, if not identified when they occur or during subsequent inspection, could lead to a loss of structural integrity under further loading. An in-situ Structural Health Monitoring (SHM) system for these structures can therefore provide a means for identifying and locating an impact event, and determining and classifying damage produced as a result of an impact (Diamanti & Soutis, 2010). In such cases, Acoustic Emission (AE) based SHM systems have shown great promise for use with composite structures. The use of a broadband sensor network can help identify impact events based on the resulting waveform response at the sensor locations and a location estimation of the impact event can be performed (Mal et. al., 2003). In addition, the received waveform responses may also be used to identify the occurrence of damage produced during the impact event. This study aims to investigate characteristics of received

waveforms resulting from damage produced during low-velocity impact, in an attempt to identify damage producing impact events as well as the types of damage produced in composite structures.

Three general damage types may be produced in composite structures from low-velocity impacts: matrix damage, delamination, and fiber breakage (Davies & Zhang, 2005). Matrix cracking is typically the first failure mode to be produced from a low-velocity impact. This type of damage is produced when the matrix material (typically an epoxy) cracks without breaking the surrounding fibers. Typically such matrix cracks are oriented parallel to the reinforcing fibers, and often follow the fiber/matrix interface. Although matrix cracking is often considered not to be critical to the integrity of a composite structure, this form of damage can lead to other failure modes, particularly delamination (Richardson & Wisheart, 1996). Delamination refers to the internal separation of laminas at their boundaries, or interfaces. Interlaminar shear and normal stresses produced by out-of-plane loading such as an impact event are a common cause of delaminations in laminated composites. Fiber breakage occurs due to locally high stresses and indentation effects. Typically, this type of damage is the most difficult to detect nondestructively and yet is of great concern for structural integrity (Richardson & Wisheart, 1996). Figure 3.1 shows these damage modes in a sectioned composite laminate following low-velocity impacting.

For AE-based damage determination and characterization, a sensor array that is attached to the outside of the composite structure can monitor large areas of the component under investigation. The use of the flexural A_o wave mode is more common than the extensional S_o since it can travel longer distances and allow for a lower sensor density.

However, at lower frequencies, these wave modes become highly dispersive, making damage determination more difficult. While the extensional S_o mode is minimally dispersive, it attenuates faster and does not propagate over longer distances (Papulak, 2012). Therefore, the A_o mode is proposed in this study for damage determination and classification. Previous research has shown that delaminations and matrix cracking produce lower frequency waveforms (50-300 kHz) and carry predominantly out-of-plane frequency components. However, fiber breakage produces more of an in-plane excitation and higher frequency waveforms (above 300 kHz) (Gutkin et. al., 2011).

This study is conducted with an objective to identify the probable impact conditions in a closely simulated work condition by varying the boundary conditions, specimen types and impact parameters under different settings of impact velocities, mass and impactor design. In addition, a predominant part of this work is to induce specific damage at particular intervals to differentiate between fiber breakage, matrix cracking and delamination. The understanding of a dynamic response of a composite structure to an impact event is of much importance for the design and modifications process.

3.3 Experimental Setup

Low-velocity impacts were performed using a variety of composite plate layups and thicknesses, support conditions, and impactor geometries in an effort to produce different formations of composite damage in the test panels. Of particular interest was producing “targeted” damage states for use in differentiating the AE waveforms produced from “matrix dominated” damage (matrix cracking and delamination) versus “fiber dominated” damage states (fiber breakage).

3.3.1 Composite Plate Fabrication

Quasi-isotropic flat composite panels of varying size and thickness were fabricated using three carbon/epoxy unidirectional prepreg materials: IM7/8552, AS4/3501 and IM7/8551 (See Appendix A, B and C for material properties). These composite materials were chosen based on their different fiber strengths and matrix fracture toughness values, which were expected to produce different damage states during low-velocity impact testing. Table 3.1 lists the dimension of the test panels and layup information using the various material types.

3.3.2 Drop Tower Impact Tester

Two drop towers were used to initiate particular damage modes in quasi-isotropic laminates to adjust varying size test plates. Each of the drop tower impact testers are further discussed.

3.3.2.1 Instrumented Drop Tower

Instrumented drop-weight impact testing was performed with a specially designed impact tower that allowed flexibility with different test panel sizes and shapes as well as with different impact energy levels and masses. The instrumented drop tower developed for this purpose is shown in Figure 3.2. The test apparatus consisted of an aluminum guide tube to contain the impact vessel during drop-weight impacting. The guide tube is attached on to the steel frame structure using U-bolts and screws. Additionally, corks are used to hold the U-bolts in place as well as to reduce friction. The impact vessel, shown in Figure 3.3a, was fabricated from UHMW polyethylene and enclosed the piezoelectric force link

and allowed for different impacting masses.

A 1 in. diameter hemispherical indenter, shown in Figure 3.4, was used to impact the composite test panels. The outer dimension of the impact vessel was selected to fit the guide tube, ensuring a proper clearance to minimize friction. An aluminum cap was also fabricated to press fit on top of the guide tube where the pulley was mounted for release/retrieval purposes. A data acquisition and cable access slot was machined in the guide tube to ensure enough slack of the cable wires during impact. The height of the impact vessel dropped was identified manually for every operation.

3.3.2.2 Instron Dynatup 8250 Drop Tower

For specific damage characterization experiments, a pneumatically-assisted Instron Dynatup 8250 HV drop tower was used to impact smaller 6 in. x 6 in. quasi-isotropic composite test panels (Instron, 1999). A manual tooth-ratchet system was used to catch the impactor after impact and prevent multiple rebounds on the test panels as shown in Figure 3.5a. The system was switched on immediately after impact to jam the tooth on to the impacting mass support to stop multiple rebounds. A spherical 0.063 in. diameter indenter (Figure 3.5b) and a conical 0.44 in. diameter indenter with a flat tip (Figure 3.5c) with total drop weights 9.38 lbs and 9.44 lbs, respectively, were used for impact experiments. Two support conditions were used: edge-clamping and a silicon rubber pad back-face support (see Figure 3.6). A National Instruments Data Acquisition System in conjunction with the Impulse Data Acquisition software were used to record the load versus time and sensor signal responses.

3.3.3 Data Acquisition System

Inside the impact vessel of the instrumented drop tower, a 26 kip piezoelectric Kistler 9372A quartz high impedance force link was used to measure the impact load (Kistler, 2003). The force link was connected to a charge mode dual amplifier Kistler Type 5010 that converted the sensor signals into proportionally controlled voltage (Kistler, 2009). Based on the level and type of damage desired, various masses were added to the impactor.

For the Instron Dynatup 8250HV drop tower, the impact tup secured onto the lower crosshead provided the load data to the Impulse Data Acquisition system (Instron, 1999). The output of the amplifier was connected to the NI data acquisition system to record load responses with the sensor signal responses.

A National Instruments (NI) PXIe-1073 data acquisition system coupled with NI LABVIEW and MATLAB scripts were used for data collection and signal processing. Prior to impacting, a mounting template was used to provide proper placement of the sensor to the test panel. Sonotech High Z-HV was used as the coupling gel to reduce impedance mismatch between the test specimen and structure and allow better signal transmission.

3.3.4 Piezoelectric Sensors

After careful analysis of sensor performance using both active and passive testing methods, two AE sensor types were selected for use in the damage characterization study based on their optimal performance on composite structures (Uprety et. al., 2014). The Digital Wave B1025T (Figure 3.7a) and Vallen Systeme 900-M (Figure 3.7b) sensors were selected for use with the instrumented drop tower, and Digital Wave's B1025T was used

for the Instron Dynatup drop tower experiments to further evaluate these sensors based on waveform analysis during low-velocity impact testing. These sensors offer a broadband operating range, high sensitivity to Lamb wave modes, ease of applicability, and a lower footprint on a test specimen (Uprety et. al., 2014).

3.3.5 Post-Impact Analysis

Ultrasonic inspection employs the use of higher frequency sound waves to determine internal damage. "Pulse-echo" ultrasonic C-scan is one of the most common types of nondestructive inspection used to identify internal damage in composite laminates, and is based on evaluating the reflected waves off of the back surface of the component (Abdel-Latif, 2009). For this study, Sonix ultrasonic inspection system was used with a 5 MHz Panametrics V309 ultrasonic transducer. As the transducer scanned the desired area of a test specimen, signals were gated to capture the back-wall reflection of the plate and identify damage occurrence, if any. Figure 3.8 shows the process of ultrasonic C-scan inspection. The test panels were scanned both pre-impact to assess the fabricated condition, and post-impact to determine the extent of damage produced. In addition, the test panels were sectioned through the impact region, polished and photographed using a Dinoxlite Digital Microscope for further post-impact damage classification. For detecting fiber breakage, sectioned regions of the test specimen containing the impact damage were subjected to a pyrolysis process referred to as "thermal deply". The sectioned regions were heated to a high temperature in the absence of oxygen to decompose the epoxy resin, and the remaining carbon fibers were inspected layer-by-layer at low magnification to identify fiber failure (Wang et. al., 2012).

3.4 Impact Testing Parameters

Preliminary impact testing was performed to investigate energy levels and boundary types required to produce the desired damage states. A back-face support condition reduces global bending deformations, and the use of a smaller diameter three-faceted indenter produces greater fiber damage in the vicinity of the impact. In contrast, an edge support condition allows for a more compliant structure, which will experience more global bending deformation during impacting and produce more delamination damage. Additionally, the use of a larger hemispherical indenter reduces the occurrence of fiber damage. Since a broad range of frequency spectrums are expected for different damage modes, a broadband AE sensor is useful to effectively record varying frequency responses created by different impact conditions.

3.4.1 Damage Formation

To investigate damage formation in composite laminates, a series of 20 in. x 20 in. x 0.208 in. quasi-isotropic $[45/0/-45/90]_{2s}$ panels were fabricated using Hexcel IM7/8552 carbon/epoxy unidirectional prepeg material. These test panels were used with a back-face support condition that included the use of a silicon rubber pad as shown in Figure 3.9a. AE sensors were attached at the center of the plate and impacting was performed at specified locations to ensure there was no damage path between the impact location and the receiving sensor (See Figure 3.9b). Using the instrumented drop tower, multiple impacts were performed equidistant from the two sensors attached at the center of the plate using a 10.91 lbs mass impactor. Tests were performed using drop heights ranging from 1 in. to 6 in., with impact energies ranging from 1ft-lbf to 5.5 ft-lbf to compare elastic impacts (no

detectable damage) to the formation of detectable damage in the test panel. The panel was ultrasonically C-scanned after each impact. This series of impacts was performed four times to ensure repeatability of the results obtained. Two sensor types were used for studying the signal behavior: Digital Wave (DW) B1025-T and Vallen Systeme (VS) 900-M.

3.4.2 Delamination with Minimal Fiber Breakage

The Instron Dynatup Tower 8250 drop tower was used with an edge-clamped boundary support condition as per ASTM Standard D7136 (ASTM, 2012), in conjunction with the spherical indenter to create delaminations in test panels with minimal fiber failure. A series of 6 in. x 6 in. Hexcel AS4/3501-6 and IM7/8551 quasi-isotropic composite laminates with a 24 ply $[0/45/90/-45]_{3s}$ layup were used. Impact energies 4.73 ft-lbf and 7.10 ft-lbf were used with an impact velocity of 55 in./sec. and 68 in./sec., respectively. Two Digital Wave B1025T sensors were placed 2 in. from the impact location to record signal waveforms. The edge clamped support structure featured a 3 in. x 5 in. opening to allow plate deflection and clamps to secure the edges of the plate during impacting. Figure 3.10a shows the impact experiment setup.

3.4.3 Fiber Breakage with Minimal Delamination

To investigate the AE signal response produced from impact damage consisting primarily of fiber damage, a series of 6 in. x 6 in. test panels of quasi-isotropic AS4/3501 and IM7/8551 carbon/epoxy were used. Low-velocity impact testing was performed using a 0.125 in. thick silicon rubber pad as the back-face support condition. The test panel was

placed flat on the rubber pad and impacted with the conical indenter with a flat tip using impact energies 2.37 ft-lbf and 4.73 ft-lbf, corresponding to impact velocities of 40 in./sec. and 55 in./sec., respectively. Two DW B1025T sensors were placed 2 in. from the impact location for data acquisition. Figure 3.10b shows the experimental setup.

3.5 Results and Discussion

Three different impact experiment conditions were performed to initiate different damage modes on to the test panel. The results of each are discussed next.

3.5.1 Damage Formation

Figure 3.11 shows the load versus time curves for three impacts performed at energy levels: 3.64 ft-lbf, 4.55 ft-lbf and 5.46 ft-lbf on the IM7/8552 quasi-isotropic test panel. At the lowest impacting energy of 3.64 ft-lbf, an elastic impact was believed to occur without the formation of any detectable damage. The load versus time curve shows a complete energy transfer between the indenter and the test specimen. At a 4.55 ft-lbf impact energy, minor load drops were observed in the ascending load curve indicating possible damage initiation. Matrix cracking was therefore believed to be the first damage mode initiated on the test panel as a result of surface indentation. For a 5.46 ft-lbf impact energy drop, sudden high amplitude load drops were observed at the 800 lbf peak load vicinity suggesting significant damage on the test specimen. The periodic load drops between 1400 and 1800 μs. were believed to have been produced by both matrix damage and possible fiber failure. Following the point of maximum loading, several additional load peaks were observed until complete unloading.

After careful observation and signal analysis, it was postulated that these force oscillations related to the manual drop process, convolved with both the harmonic response of the system as well as the structure response to the impact event. These responses were observed to increase for compliant boundary conditions and higher impact energy experiments.

For the AE-based identification of damage formation, the load versus time curve was compared to the AE signal responses received using both the DW B1025T and VS 900-M sensors. Figure 3.12a shows the received raw AE signal using DWB1025T sensor and Figure 3.12b shows the received raw AE signal using the VS900-M sensor for all three impact events. The two lower energy impacts, 3.46 ft-lbf and 4.55 ft-lbf, showed no indications of damage formation in the received signals using the two sensor types. For the 5.46 ft-lbf impact, several high-frequency components were observed in the sensor signal between 1400 – 2000 μs, indicating multiple formations or propagations of damage within the specimen.

For further analysis of the damage events, the spectral responses of these received signals were characterized using Fast Fourier Transform (FFT) and MATLAB code scripts. Figure 3.13 shows the FFT response for sensor signals from all three impacts. The FFT of the received signals showed a general flat response for the 3.64 ft-lbf and 4.55 ft-lbf impacting energies event, conforming to the signal events indicating no damage formation. For the 5.46 ft-lbf energy impact, a higher range of signal energies at frequencies below 500 kHz were observed suggesting multiple damage formations. Coupled with the time-matched load drop and waveform response, it is believed that the formation of possibly different damage modes: matrix damage, delamination, and possibly fiber failure created

these signals. Note that the DW B1025T sensor provides a wider frequency spectrum (1 kHz - 1.5 MHz) versus the VS 900-M sensor (100 kHz – 900 kHz) and therefore the larger peaks below 100 kHz are only observed using the VS 900-M sensors.

3.5.2 Delamination with Minimal Fiber Breakage

The use of edge-clamped support condition allowed for greater global deformation of the test panel, therefore causing more delamination damage as opposed to localized damage (including fiber breakage) at the impact location. Figure 3.14 compares the load versus time response for these two types of carbon/epoxy composite materials impacted at two different energy levels. For both impact energy levels, the IM7/8551 material exhibits higher load levels in comparison to the AS4/3501 material. For an impacting energy of 3.13 ft-lbf, an elastic load-time curve was observed for the IM7/8551 panel, indicating no damage to the test specimen. In contrast, the AS4/3501 test panel exhibited a sudden load drop at 500 lbf, indicating damage to the test specimen, which was believed to be delamination damage. Multiple load amplitude oscillations were observed following the initial load drop representing random delamination propagation within the test structure. Further load drops along the line were indicative of matrix damage. At the 4.69 ft-lbf impacting energy, the IM7/8551 test panel showed slight evidence of damage as the load peaked at 910 lbf, believed to be matrix damage. In contrast, the AS4/3501 test panel showed evidence of both delamination and matrix damage events occurring, and reached a significantly lower peak load.

Figure 3.15 shows the AE response signals recorded using the DW B1025T sensor for the two impacting energies on the AS4/3501 test plate corresponding to the load versus

time curve. Further spectrograms showing the frequency content of received signal at the impact frame are also shown. The test plates were cut through the center of the impact and microscopically investigated; the images are shown alongside the C-scan pictures of the impact location. The AE response and further evaluations of the IM7/8551 test panel are shown in Appendix H. For the AS4/3501 test specimen, the received signals as well as the spectrograms showed a sharp high amplitude response signal component around 2.5 ms and 1.8 ms for the 3.13 ft-lbf and 4.69 ft-lbf impacting energies, respectively. At both impacting energies, the time-frequency domain of the signal analysis showed lower high density signals at a peak at 13.11 kHz for the loading curve before damage was initiated. For the IM7/8551 test panel, the elastic loading frequency changed to 15.64 kHz regardless of the impacting energy. As shown in Figure 3.15, at the point of delamination initiation at high amplitude AE, the frequency content of the signal ranged up to 150 kHz for both impacting energies. Furthermore, the ultrasonic C-scan of the AS4/3501 test specimens as well as microscopic investigation of the sectioned specimen showed significant delaminations comparable to the impactor diameter. With increasing impact energy, the delamination amplitude AE and damage size were almost doubled. As shown in Appendix H for the IM7/8551 test panel, minimal matrix cracking of lower frequency content (80 kHz) was observed owing to its higher fracture toughness.

3.5.3 Fiber Breakage Dominated

For the back-face support condition, minimal deflection was possible and thus more localized damage formation was observed from impacting. Figure 3.16 compares the load versus time curves from two drop heights for both AS4/3501 and IM7/8551 test panels.

Again, higher load responses were recorded for the IM7/8551 material in comparison to the AS4/3501 test panel. In comparison to the edge-clamped support condition, the maximum load responses were lower for the back-face support due to its rigidity. For the AS4/3501 panel at a 1.57 ft-lbf and 3.15 ft-lbf impacting energies, an initial rapid load drop at 470 lbf was observed, similar to the load level from the edge-clamped support condition discussed previously. Additionally, large load amplitude oscillations were observed for the back-face support condition, indicating further damage in addition to delamination and matrix damage. The multiple load drops around the peak load region are indicative of fiber breakage. For IM7/8551 test panel, however, at an impacting energy of 1.57 ft-lbf, a comparable elastic load curve was observed with minor load drops which indicated matrix breakage to the test specimen. At the 3.15 ft-lbf impacting energy, multiple damage events around the peak load of 810 lbf were observed that could be representative of fiber breakage. In contrast to delamination-dominated impact experiments, several load drops were observed early on in the load-time curve suggesting surface damage following impact. The load drops continued to increase until the peak displacement of the test panel and the load amplitude oscillations were constantly scattered suggesting several intraply damage with minimal delaminations and higher stiffness reduction of the structure.

Figure 3.17 shows the raw AE signals recorded for impacts at 1.57 ft-lbf and 3.15 ft-lbf energies for the AS4/3501 test panel corresponding to the load-time curve. In addition, a time-frequency domain spectrogram and post-impact analyses using C-scan and digital microscope are also shown. The impact analyses results on the IM7/8551 material type are shown in Appendix I. At both the impacting energies, a concentration of higher frequency components was observed between 1 ms – 3 ms, indicating multiple damage

mode formation on the test structure. Again, in accordance with the delamination-dominated experiments, the time-frequency domain of the elastic AE signal analysis showed peak frequency at 13.11 kHz and 15.64 kHz for the AS4/3501 and IM7/8551 test panel, respectively. At an initial loading time of approximately 0.75 ms, a sudden increase of the signal amplitude was observed which suggested delamination initiation in addition to other damage modes. In contrast to the delamination dominated responses, the amplitude spectrogram showed a much higher frequency content of the AE signals up to 350 kHz for the 1.57 ft-lbf and 500 kHz for the 3.15 ft-lbf impacting energies, respectively. Such higher magnitude AE responses were further indicative of fiber failure in the test panel. Ultrasonic C-scan results on the AS4/3501 test panel showed fiber breakage with multiple delaminations which were further confirmed with the microscopic investigation. The damage sizes on the test panels were 0.5 in. and 0.65 in., closely correlating to the indenter size.

It is believed that the flat tip of the conical impactor head caused higher surface indentation before penetration therefore causing subsurface delamination in addition to fiber breakage. As shown in Appendix I for the IM7/8551 test panel, only limited matrix damage was observed for the 1.57 ft-lbf impact energy with frequency content up to 50 kHz. At a higher impacting energy of 3.15 ft-lbf, the amplitude spectrogram of the signal suggested matrix damage at around 80 kHz whereas higher energy signals around 380 kHz suggested fiber breakage. Some observations of surface fiber damage at the impact location could be inferred from the C-scans, but no definitive conclusions could be made without further investigations using the thermal deply process to burn off the excess resin and perform each ply evaluation.

3.6 Summary and Conclusions

Low-velocity impact experiments were performed on quasi-isotropic composite test panels at different energy levels to initiate specific damage types on the test specimen. An instrumented drop tower was used to perform testing using larger composite panels with a back-face support conditions to understand the AE signal response for elastic and damage-producing impacts. Follow-on impact testing was performed to initiate specific damage types using smaller composite test panels. AE signal responses were collected during impacting and the test panels were ultrasonically C-scanned after impact to identify the internal damage produced. Additionally, the impacted panels were sectioned through the impact region and microscopically investigated to identify the damage present.

Both load versus time curves and AE signal responses showed good correlation with identified damage modes produced in the test panels. Edge-clamped and back-face support conditions both showed matrix damage as the first failure mode, typically near the peak load, and corresponding to frequency ranges less than 100 kHz. These damage signals were not easily identifiable in the AE sensor signal responses and thus inspection of the sectioned specimen using a microscope was required. For the edge clamped delamination-dominated test condition, greater delamination areas were produced due to the global panel deflection. High frequency components in the AE sensor signal responses were produced in the AS4/3501 composite test panels that corresponded in time with a dramatic load drop followed by higher load amplitude oscillations. Additionally, ultrasonic C-scans and microscopic investigation showed several interply delaminations. In contrast, the IM7/8551 test panels experienced only matrix damage. For the back-face supported fiber breakage-dominated test condition, a combination of damage modes were produced in the

AS4/3501 test panels, including matrix damage, delamination, and fiber breakage. Frequency ranges of the recorded AE sensor signals were as high as 500 kHz for the damage modes produced. For the IM7/8551 material, the occurrence of matrix damage produced a visible load drop on the load-time curve. Although the presence of delamination was not clearly evident, the higher frequency range of up to 380 kHz suggested fiber breakage had occurred. Further investigation with the thermal deply process is ongoing to effectively identify the damage modes produced. It was also observed that the elastic impact signal corresponding to the loading curve with no visible damage showed the same peak frequency with varying smaller peaks. Therefore, it is suggested that the elastic impacts are independent of the impacting energy and test boundary conditions and are solely a function of material type, thickness and properties. Further testing to conform to these observations is recommended with complex composite structures and varying boundary conditions.

It is recommended that the higher fracture toughness IM7/8551 material be used for further back-face support testing where fiber damage is desired with minimal matrix damage or delamination. In addition, a thicker test specimen in conjunction with a thinner silicone rubber pad could further constrain global plate deflection and provide for a more rigid support condition to produce a damage state consisting primarily of fiber breakage. Additionally, the lower facture toughness of the AS4/3501 material as well as the use of an edge-clamped support condition and a thinner test panel are well-suited for producing matrix-damage dominated damage states during impacting.

This study shows promising results on identifying the occurrence and type of damage produced in composite laminates using surface-bonded AE sensors. Further

damage identification and characterization experiments and analyses are ongoing to incorporate multiple sensor types for performance assessment for use in impact location estimation. Larger test panels with best-suited boundary conditions are recommended for use to avoid reflections from panel edges and better identify sensor responses corresponding to specific damage modes in composite structures.

3.7 Acknowledgment

This work is supported in part by the National Aeronautics and Space Administration (Award No. NNM13AA12G) and the Air Force Office of Scientific Research (Award No. FA95501210291).

3.8 References

Abdel-Latif, A. M. (2009). An overview of the applications of NDI/NDT in engineering design for structural integrity and damage tolerance in aircraft structures. *Damage and Fracture Mechanics: Failure Analysis of Engineering Materials and Structures*, 93-100. AIQ-ICF Proceedings. 2009

American Society for Testing and Materials. (2012). *Standard test method for measuring the damage resistance of a fiber-reinforced polymer matrix composite to a drop-weight impact event*. ASTM International.

Davies, G. A., & Zhang, X. (1995). Impact damage prediction in carbon composite structures. *International Journal of Impact Engineering*, *6*(11), 149-170.

Diamanti, K., & Soutis, C. (2010). Structural health monitoring techniques for aircraft composite structures. *Progress in Aerospace Sciences*, *46*(8), 342-352.

Gutkin, R., Green, C. J., Vangrattanachai, S., Pinho, S. T., Robinson, P., & Curtis, P. T. (2011). On acoustic emission for failure investigation in cfrp: Pattern recognition and peak frequency analyses. *Mechanical Systems and Signal Processing*, *11*, 1393-1407.

Instron Corporation. (1999). Instron dynatup 8250 drop weight impact tester user manual.

Kistler Instrument Corporation. (2003). *Quartz type 9301b ... 9372a high impedance, charge mode force links*. NY.

Kistler Instrument Corporation. (2009). C*harge amplifier type 5010b dual mode charge amplifier with piezotron® operating mode*. NY.

Mal, A. K., Shih, F., & Banerjee, S. (2003). Acoustic emission waveforms in composite laminates under low-velocity impact. *Proc. SPIE 5047, Smart Nondestructive Evaluation and Health Monitoring of Structural and Biological Systems II,* 1-12.

Papulak, T. S. (2012). *An inverse acoustical phased array technique for impact detection and location* (Master's thesis, University of Utah).

Richardson, M. O., & Wisheart, M. J. (1996). Review of low-velocity impact properties of composite materials. *Composites Part A-Applied Science and Manufacturing*, *27*(12), 1123-1131.

Uprety, B., Kim, S., Mathews, V. J., & Adams, D. O. (2014). A comparative evaluation of piezoelectric sensors for acoustic emission based impact location estimation and damage classification in composite structures. *AIP Conference Proceedings, Annual Review of Progress in QNDE*, Boise, Idaho.

Wang, S., Zhang, W., Yang, M., & Chen, Y. (2012). The application of thermal deplying technology on the resin matrix composite damage analysis. *Advanced Materials Research*, 503-504, 148-151.

Table 3.1. Test Specimen Information.

Material type	Layup	Ply thickness (in)	Total no. of plies	Plate Dimension (in)
IM7/8552	[45/0/90/-45]2s	0.013	16	20 x 20 x 0.208
AS4/3501	[0/45/90/-45]3s	0.0052	24	6 x 6 x 0.125
IM7/8551	$[0_2/45_2/90_2/-45_2]s$	0.0056	24	6 x 6 x 0.134

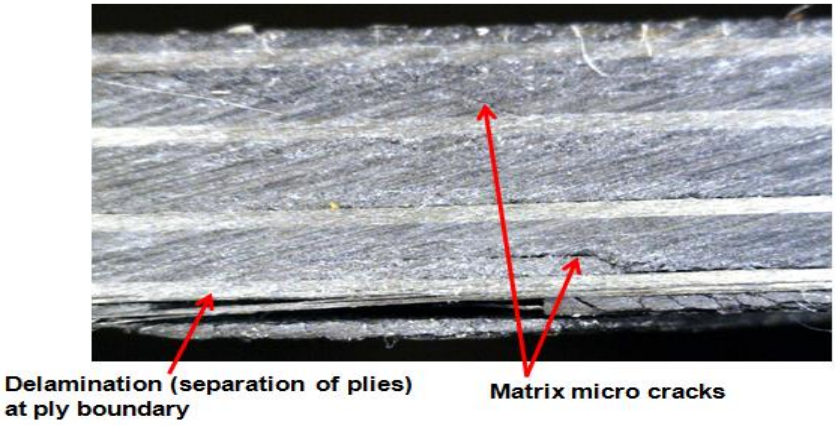

Figure 3.1. Microscopic Investigation of Composite Plate Showing Damage Modes.

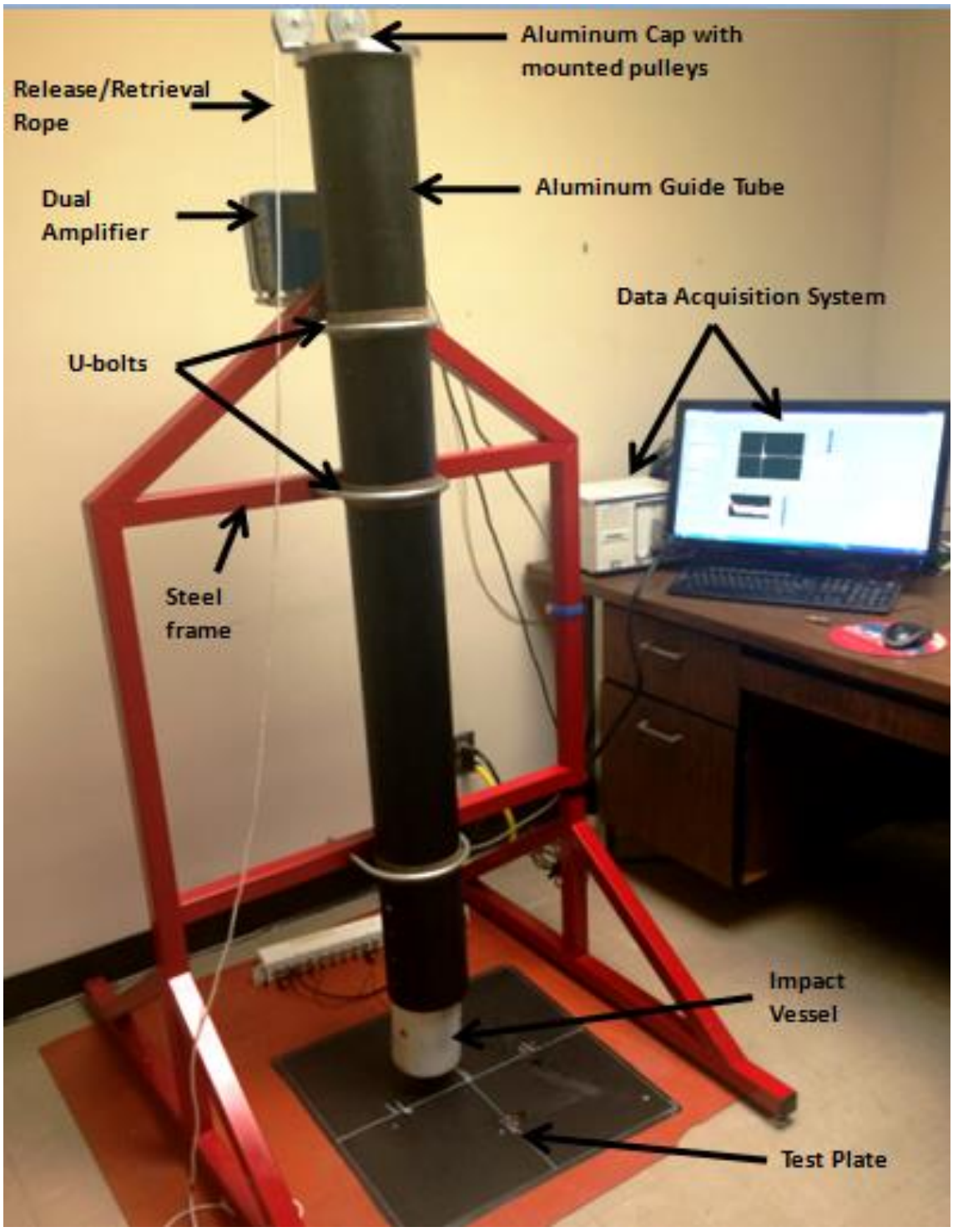

Figure 3.2. Instrumented Drop Tower Setup.

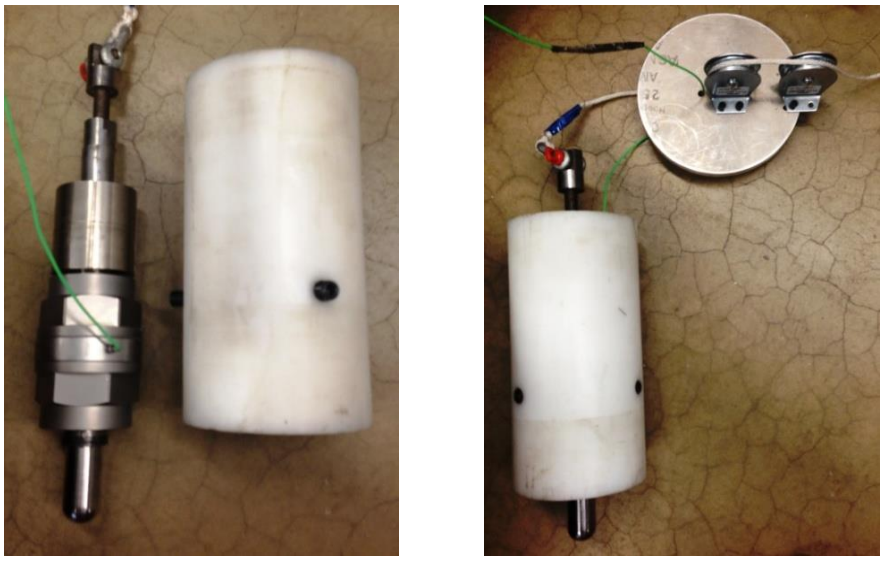

(a) (b)

Figure 3.3. Impactor Setup (a) Impact Indenter (left) and Impact Vessel (Right). (b) Enclosed Impact Vessel.

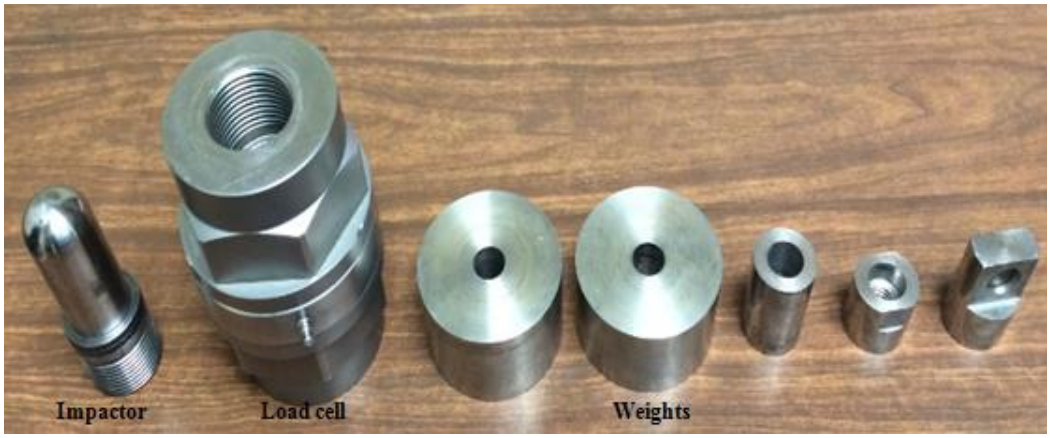

Figure 3.4. Impact Indenter Parts.

(a) (b) (c)

Figure 3.5. Indenter Mechanisms (a) Tooth-Ratchet System (b) Spherical Indenter (c) Conical Indenter.

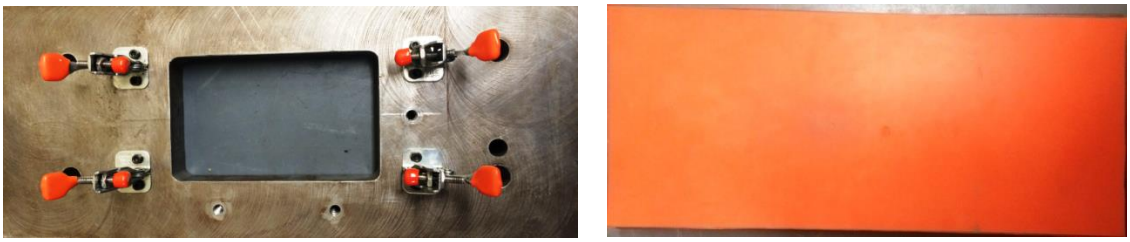

(a) (b)

Figure 3.6. Impact Process Setup (a) Edge-Clamped Rigid Structure with a 3 in x 5 in opening (b) Silicon Rubber Pad.

(a) (b)

Figure 3.7. Sensors used (a) DW B1025T Sensor (b) VS 900-M Sensor.

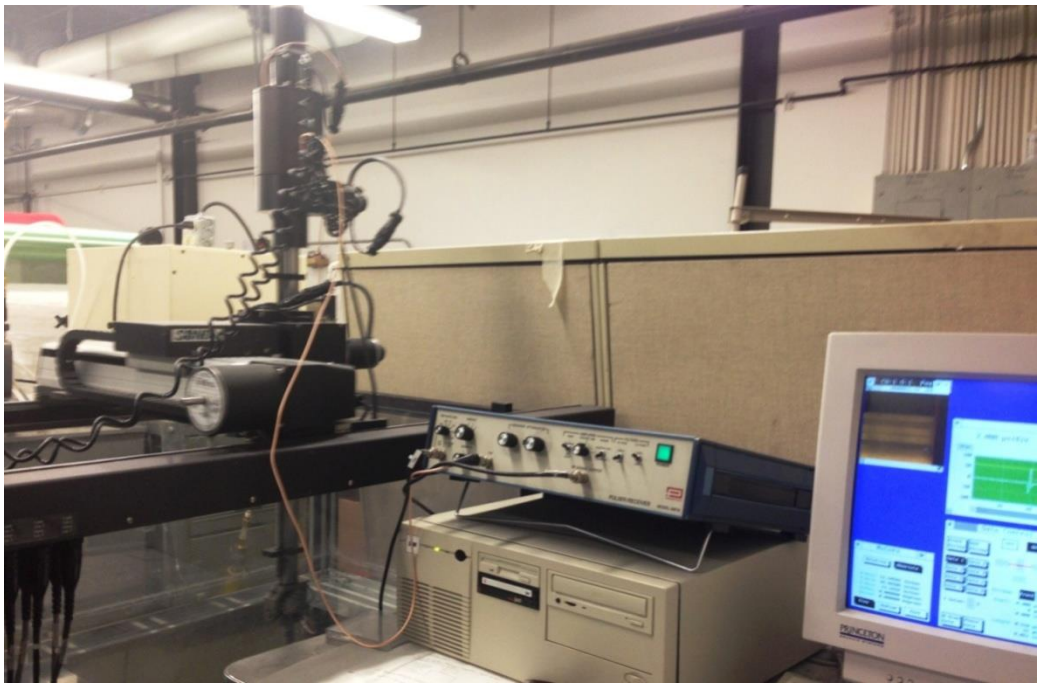

Figure 3.8. Process Setup of Ultrasonic C-scan Testing.

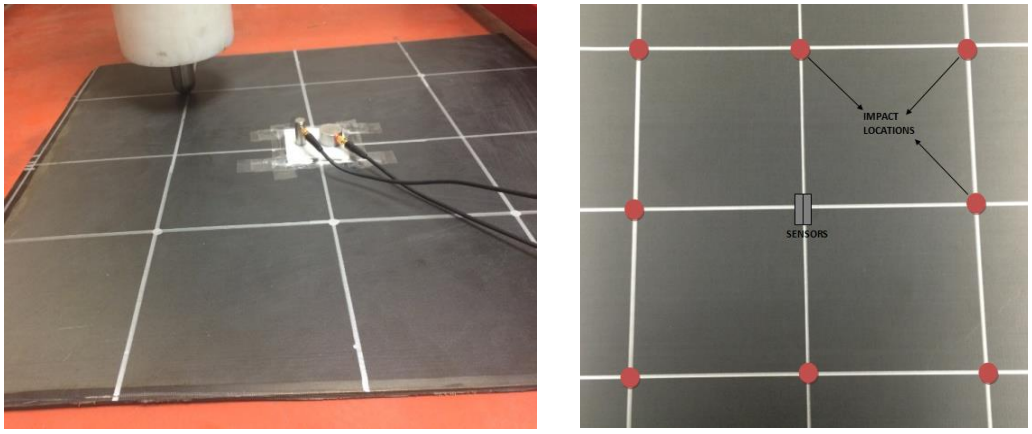

(a) **(b)**

Figure 3.9. Impact Conditions (a) Back-Face Support Condition (b) Impact Locations

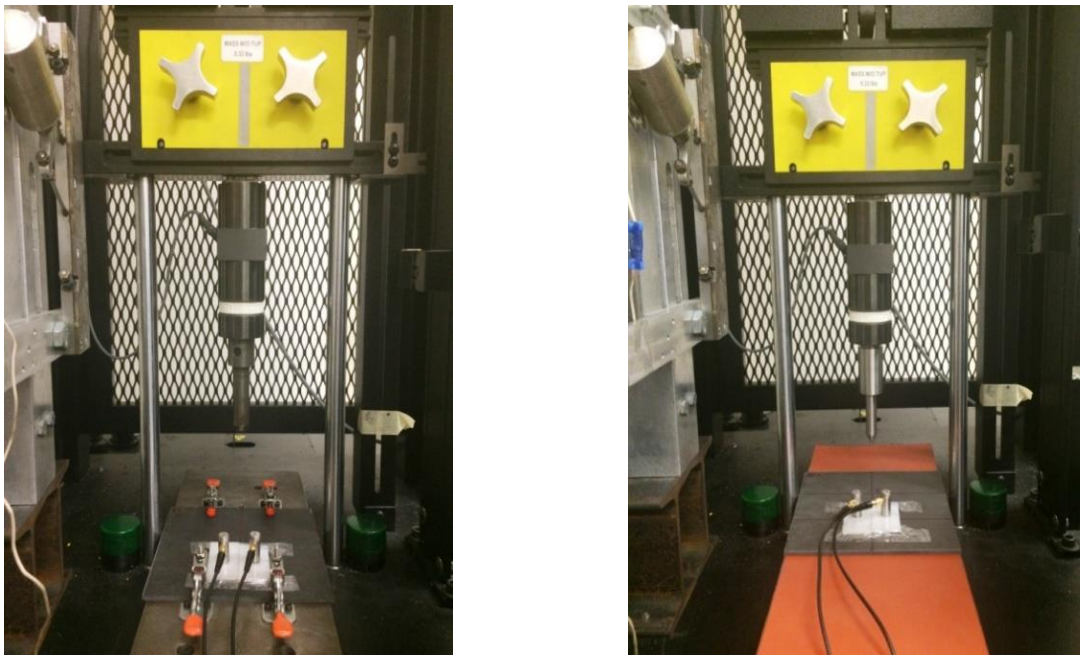

(a) (b)

Figure 3.10. Test Setup (a) Edge-Clamped Condition (b) Back-Face Supported Condition.

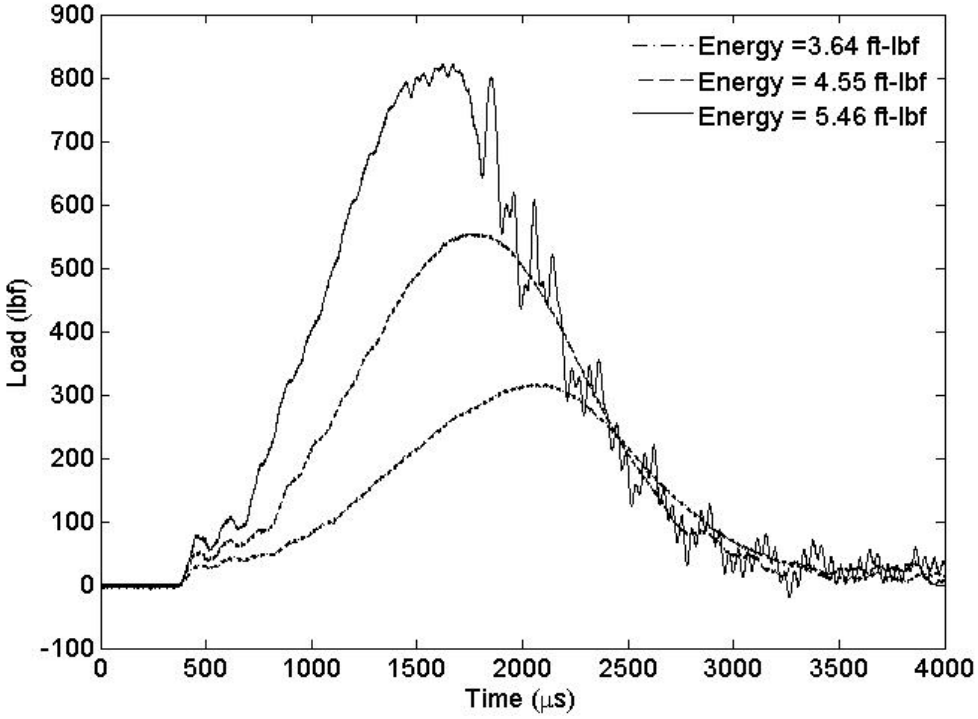

Figure 3.11. Load vs. Time Curve for IM7/8552 Impact Testing.

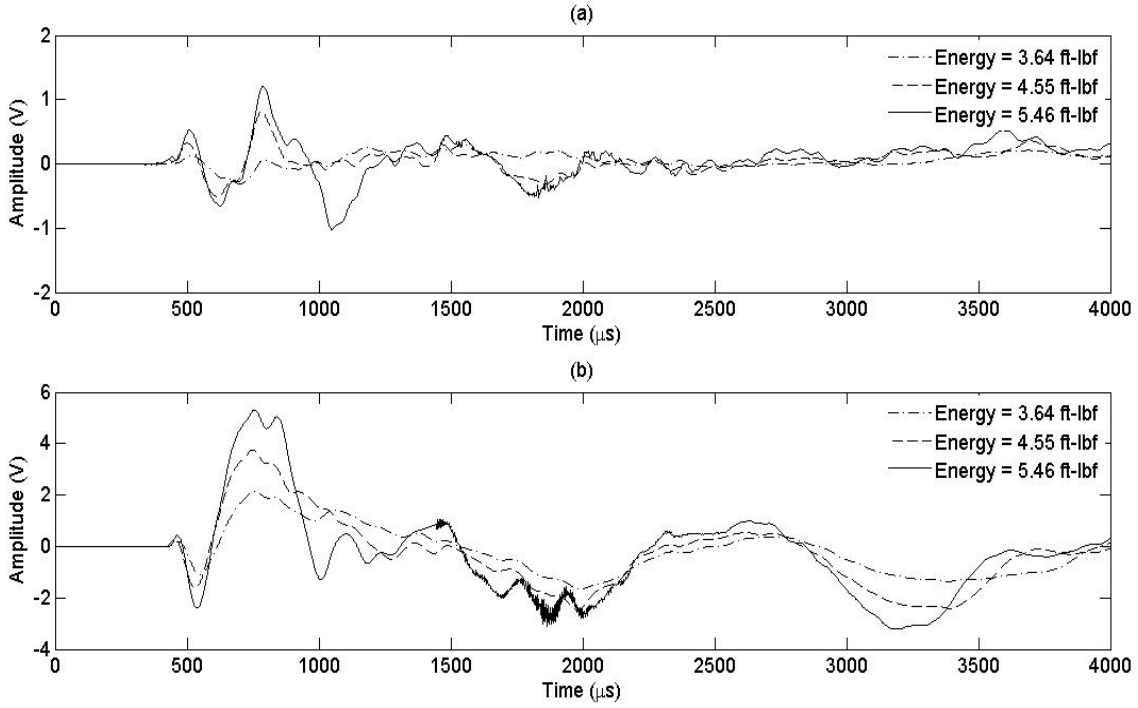

Figure 3.12. Signal Response Using (a) DW B1025T Sensor (b) VS 900-M Sensor.

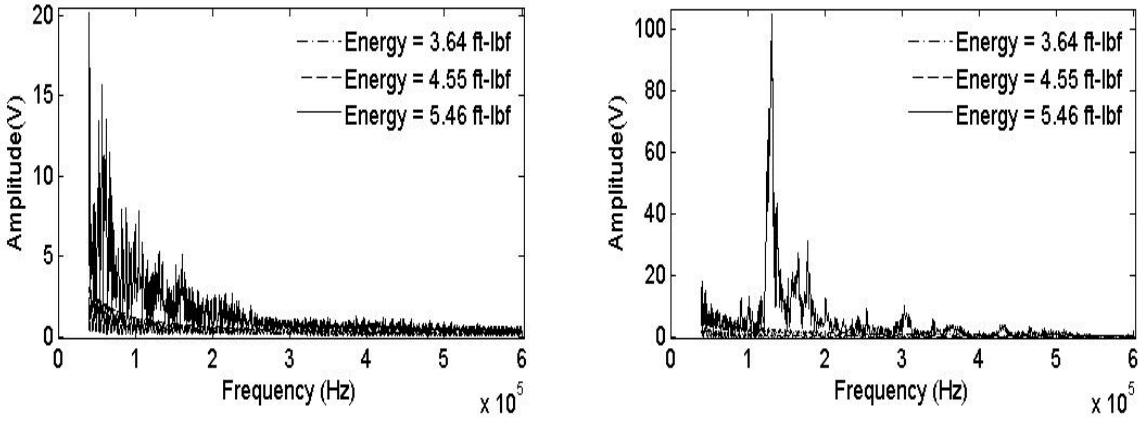

(a) **(b)**

Figure 3.13. Fast Fourier Transform of Received Signal (a) DW B1025T Sensor (b) VS 900-M Sensor.

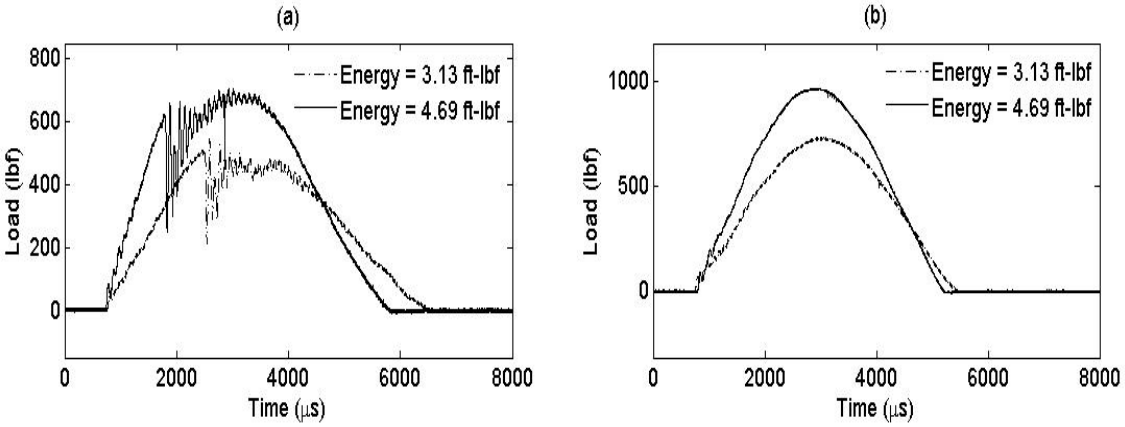

Figure 3.14. Load vs. Time Curve (a) AS4/3501-6 (b) IM7/8551.

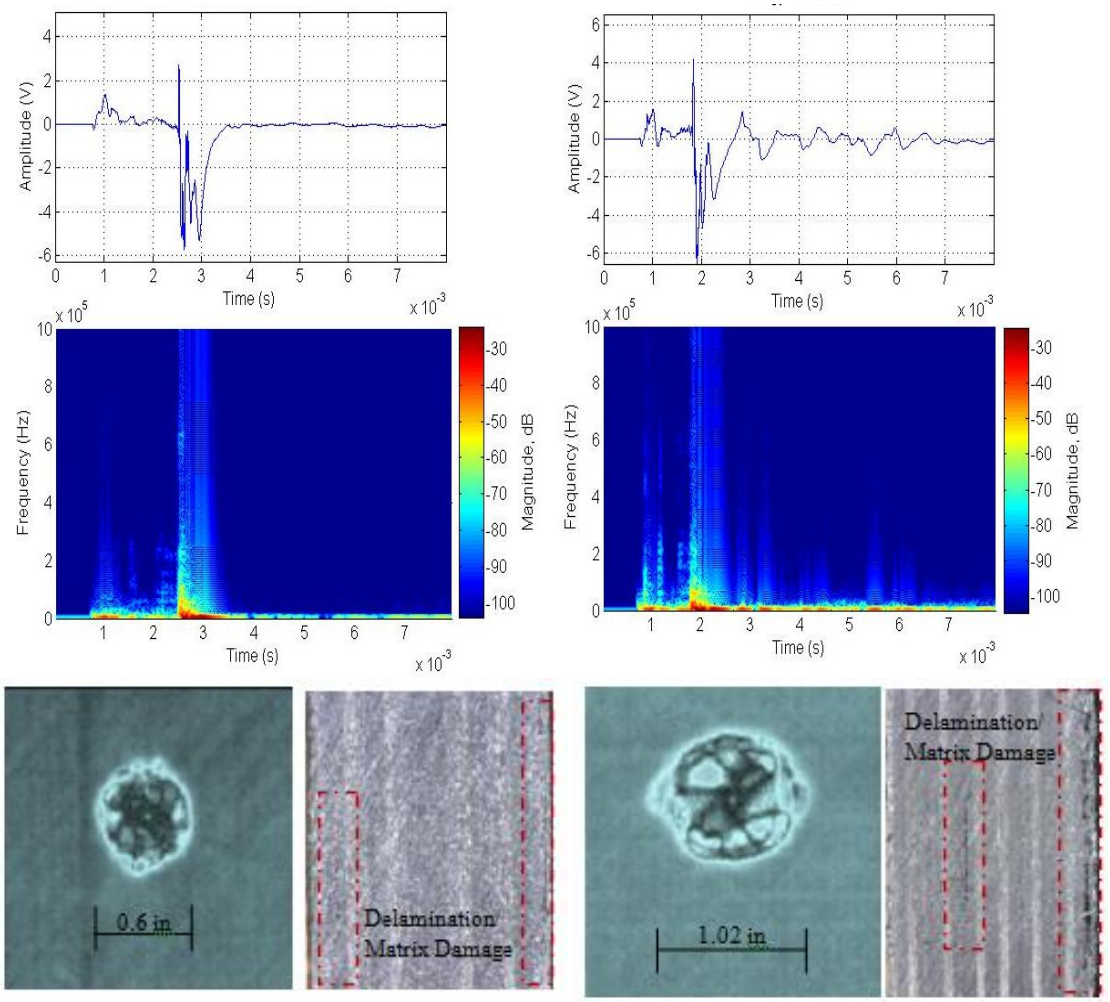

(a) **(b)**

Figure 3.15. Signal Response, Amplitude Spectrogram and Scan Results for AS4/3501 Material Type Using Impact Energies (a) 3.13 ft-lbf (b) 4.69 ft-lbf.

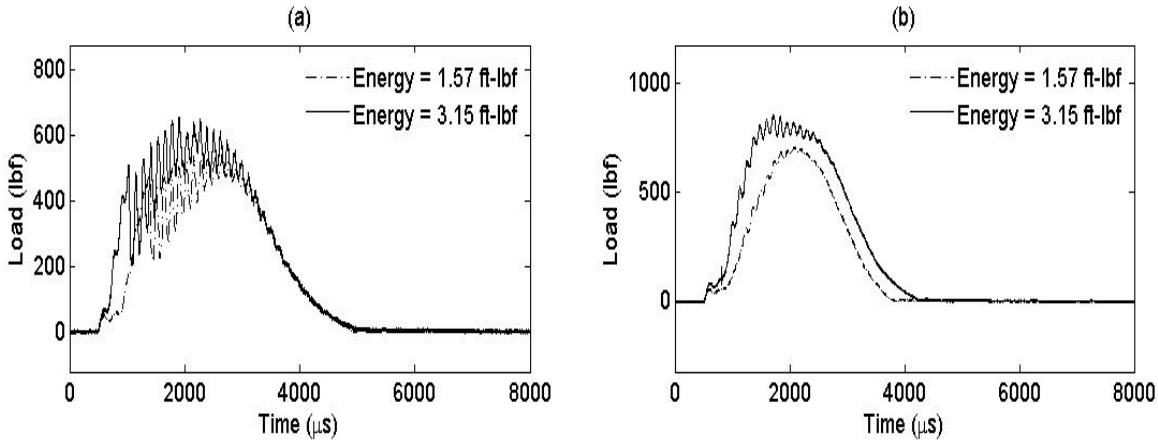

Figure 3.16. Load vs. Time Curve (a) AS4/3501-6 (b) IM7/8551.

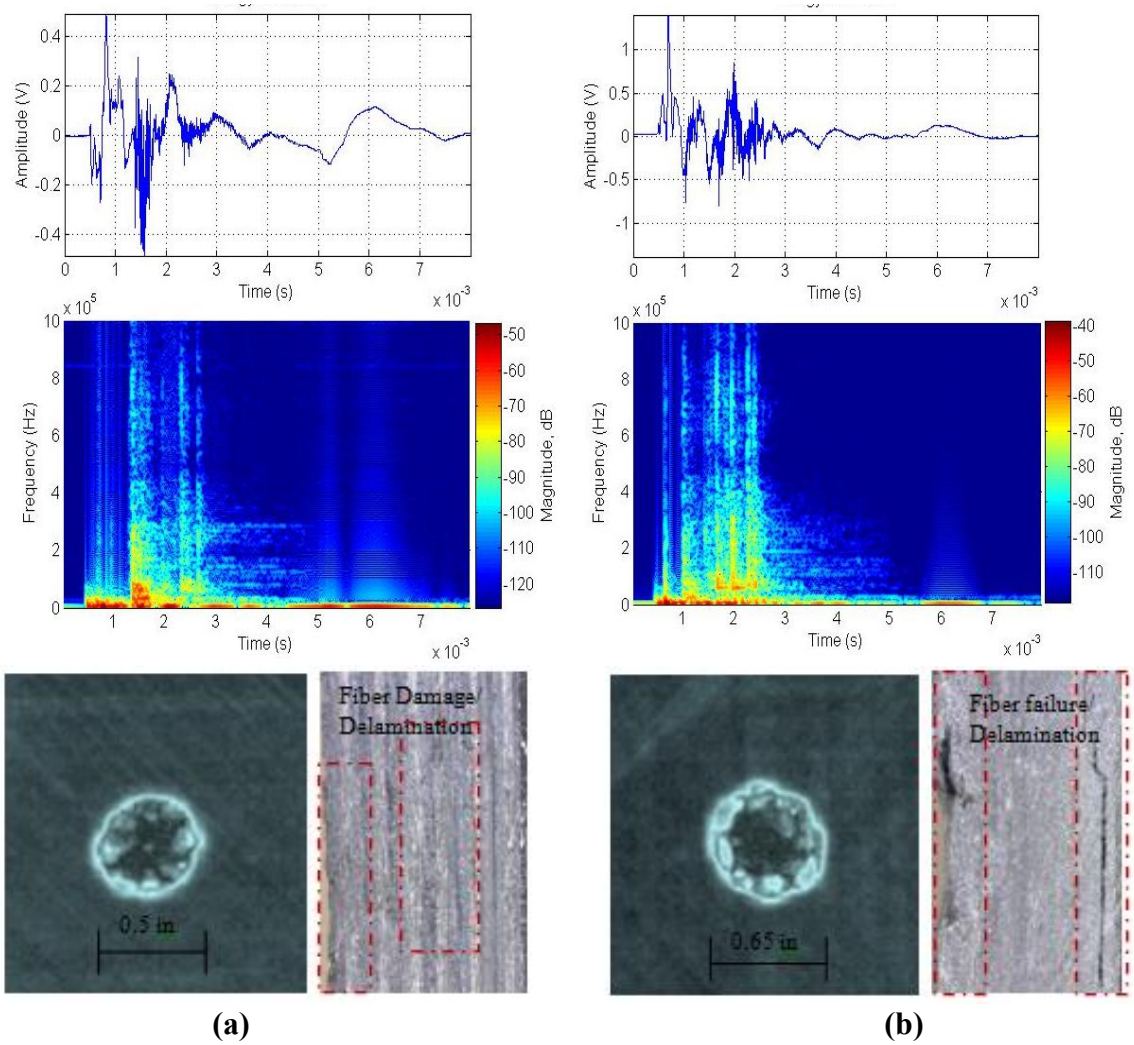

Figure 3.17. Signal Response, Amplitude Spectrogram and Scan Results for AS4/3501 Material Type Using Impact Energies (a) 1.57 ft-lbf (b) 3.15 ft-lbf.

CHAPTER 4

CONCLUSION AND FUTURE WORK

4.1 Conclusion

While impact damage assessment and type classification in composite structures remains a challenging field of study in structural health monitoring, preliminary sensor evaluation and damage type initiation and characterization were successfully demonstrated in this study. A comparative study of six commercially available piezoelectric AE sensors was performed using both active and steel ball drop testing methods to assess their performance in plate wave mode detection, and received signal quality using aluminum and composite panels. In general, wave modes received in quasi-isotropic composite panels showed higher wave propagation dispersion to changing frequencies due to their multi-laminated plate structure in comparison to the isotropic aluminum panels. For active testing, wave mode velocities of S_o and A_o modes were found to be in good agreement with the predicted values using Disperse code and Finite Element Analysis methods. For steel ball drop testing, dominant A_o mode component for out-of-plane displacement was observed for all sensor types. Also, higher signal attenuation was observed in composites compared to the aluminum panel. For a low sensor footprint on the structure with optimal performance, high signal strength and broad band frequency response, four sensor types: Acellent's Single Smart Layer, Vallen Systeme's 900-M, Digital Wave's B1025T and

STEMiNC's Wire Lead sensors were recommended for further study using low-velocity impact experiments.

Furthermore, characterization of AE signals received during damage initiation on quasi-isotropic composite structures was conducted using specialized drop-weight impact experiments to produce two particular damage states: delamination-dominated and fiber-breakage dominated. Digital Wave's B1025T and Vallen Systeme's 900-M sensors were used for signal waveform recording using the NI data acquisition system along with a load cell to collect impact force data. Considerations in producing the desired damage states included the type of composite material, the laminate thickness, boundary conditions during impacts, and the geometry of the impactor. A series of 16-ply quasi-isotropic AS4/3501 and IM7/8551 test panels was fabricated and impacted at different energy levels. For a delaminated-dominated test condition, an edge supported boundary condition was used to allow plate deformation and impacts with spherical tup minimized local fiber damage on the specimen. For a fiber-breakage dominated test condition, a back-face supported boundary condition was used to reduce plate compliance and a impacts with a conical tup allowed localized fiber breakage with minimal delaminations. Post-impact inspections of the panels were done using ultrasonic scanning and sectioning with photomicroscopy. The received signals were assessed in terms of the load-time curve, amplitude response, frequency components and energy content to identify and characterize nondamage event and damage-producing impact events. For impact energies below 5 J, an elastic load-time curve was observed suggesting a complete energy transfer between the impactor and test panel and indicating minimal to no damage. Furthermore, the acoustic response of the AE signals showed elastic impact event of frequency components less than

20 kHz. It is suggested that the elastic AE was independent of the impact energy properties and boundary conditions, and changed with material type and thickness only. This frequency was therefore used as a parametric threshold for damage identification. Post-impact inspection confirmed no detectable damage on the test panels. For both delamination-dominated and fiber breakage-dominated test conditions, matrix cracks were believed to be the first damage type detected, and was characterized with low energy and frequency components of up to 80 kHz. For the delamination-dominated impact experiments, the recorded load signals showed longer contact duration of impact due to the global deformation of the test panel. The load-time curve showed dramatic load drops at particular instances of time followed by multiple random load amplitude oscillations indicating random delamination propagations within the test panel. This result correlated with the received AE signals where high amplitude responses were recorded at the same time of the first dramatic load drop. Additionally, the time-frequency domain assessment showed these damage signals carried some low frequency components (below 200 kHz) representing stiffness reduction of the test structure. Post-impact inspection with C-scans and digital microscopy confirmed several though-thickness delaminations in the test panel. For the fiber-damage dominated impact experiments, the flat tip of the conical impactor tup allowed predominant surface indentation causing partial delaminations along with fiber damage on the test panel. The impactor-panel showed shorter contact duration due to a stiff back-face boundary condition that restricted the plate movement. In contrast to delamination-dominated impact experiments, several load drops were observed early on in the load-time curve suggesting surface damage following impact. The load drops continued to increase until the peak displacement of the test panel and the load amplitude oscillations

were constantly scattered suggesting several intraply damage with minimal delaminations and higher stiffness reduction of the structure. The acoustic responses corresponding to the load-time curve showed an amplitude response of the damage signal much lower in comparison to the data observed for the delamination-dominated impact experiments. Further assessment of the damage signal in the time-frequency domain showed both low and high frequency components up to 450 kHz, representing both matrix damage and fiber breakage, respectively. Post-impact inspections showed dominant fiber breakage with some delaminations on to the test structure with fiber breaks well within the delamination area. Further processing of impact laminates using the deply method is recommended to definitively characterize the fiber failure specifications. In general, a rigid back-face support condition with a thicker test laminate is recommended for further testing to create fiber failures specifically without any interply separation.

4.2 Future Work

There are several opportunities for future work related to this study to enhance acoustic emission sensor study and damage type classification in composite laminates. Among the four proposed sensor candidates, further low-velocity impact experiments are ongoing to assess the signal responses and effectively evaluate sensor performance for use in impact location estimation algorithm. In addition, instrumented drop-tower testing with larger test plates and boundary conditions are to be studied to essentially understand signal waveform propagation with minimal reflection or interference off of plate boundaries. In doing so, further research could focus on understanding the existence and effect of back-wall reflection of thin composite and aluminum plates for better knowledge of signal

transmission on damage type analysis. Therefore, the study of plate wave modes and damage type acoustic propagation can provide a vital role in impact location estimation analyses. In addition, it is also essential to improve the acoustic sensors usage for optimal performance as well as pre- and post-impact analysis procedures for technical as well as commercial feasibility. Finite element analysis and damage modeling remain a topic of high interest and applicability for SHM study in composite structures and needs to be evaluated to simulate real-time impact conditions. Furthermore, a major area for research works should focus on damage mapping with intricate and substructures in composite plates including sandwich panels, cutouts, internal disbands as well as stiffeners for damage type classification and impact location estimation.

APPENDIX A

AUTOCLAVE CURING AND MATERIAL PROPERTIES OF AS4/3501

A.1 Material Property:

Material Property	Value
E_{11} (Pa)	1.27 E+11
E_{22} (Pa)	1.12 E+10
E_{33} (Pa)	1.12 E+10
G_{12}(Pa)	6.55 E+09
G_{13}(Pa)	6.55 E+09
G_{23}(Pa)	3.64 E+09
ν_{12}	2.78 E-01
ν_{13}	2.78 E-01

A.2 Autoclave Curing Process:

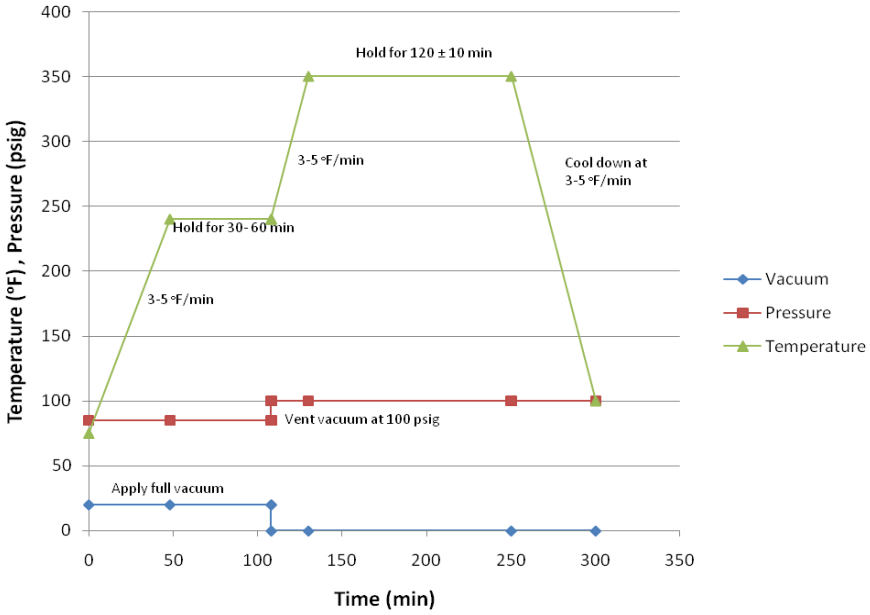

APPENDIX B

AUTOCLAVE CURING AND MATERIAL PROPERTIES OF IM7/8551

B.1 Material Property:

Material Property	Value
E_{11} (Pa)	1.66 E+11
E_{22} (Pa)	8.56 E+09
E_{33} (Pa)	8.56 E+09
G_{12}(Pa)	5.60 E+09
G_{13}(Pa)	5.60 E+09
G_{23}(Pa)	2.94 E+09
ν_{12}	2.69 E-01
ν_{13}	2.69 E-01

B.2 Autoclave Curing Process:

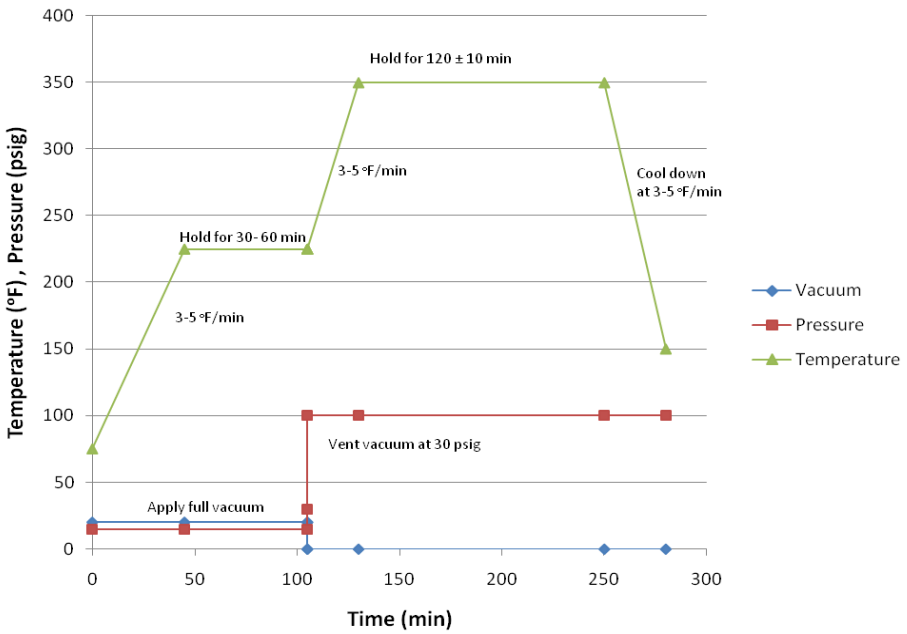

APPENDIX C

AUTOCLAVE CURING AND MATERIAL PROPERTIES OF IM7/8552

C.1 Material Property:

Material Property	Value
E_{11} (Pa)	1.71 E+11
E_{22} (Pa)	9.08 E+09
E_{33} (Pa)	9.08 E+09
G_{12}(Pa)	5.29 E+09
G_{13}(Pa)	5.29 E+09
G_{23}(Pa)	3.97 E+09
ν_{12}	3.2 E-01
ν_{13}	3.2 E-01

C.2 Autoclave Curing Process:

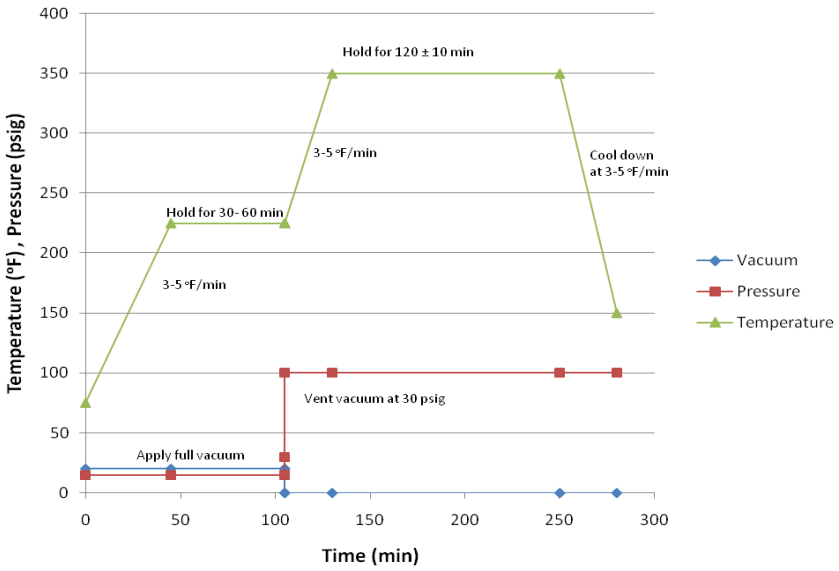

APPENDIX D

ACTIVE TESTING RESULTS ON COMPOSITE PLATE

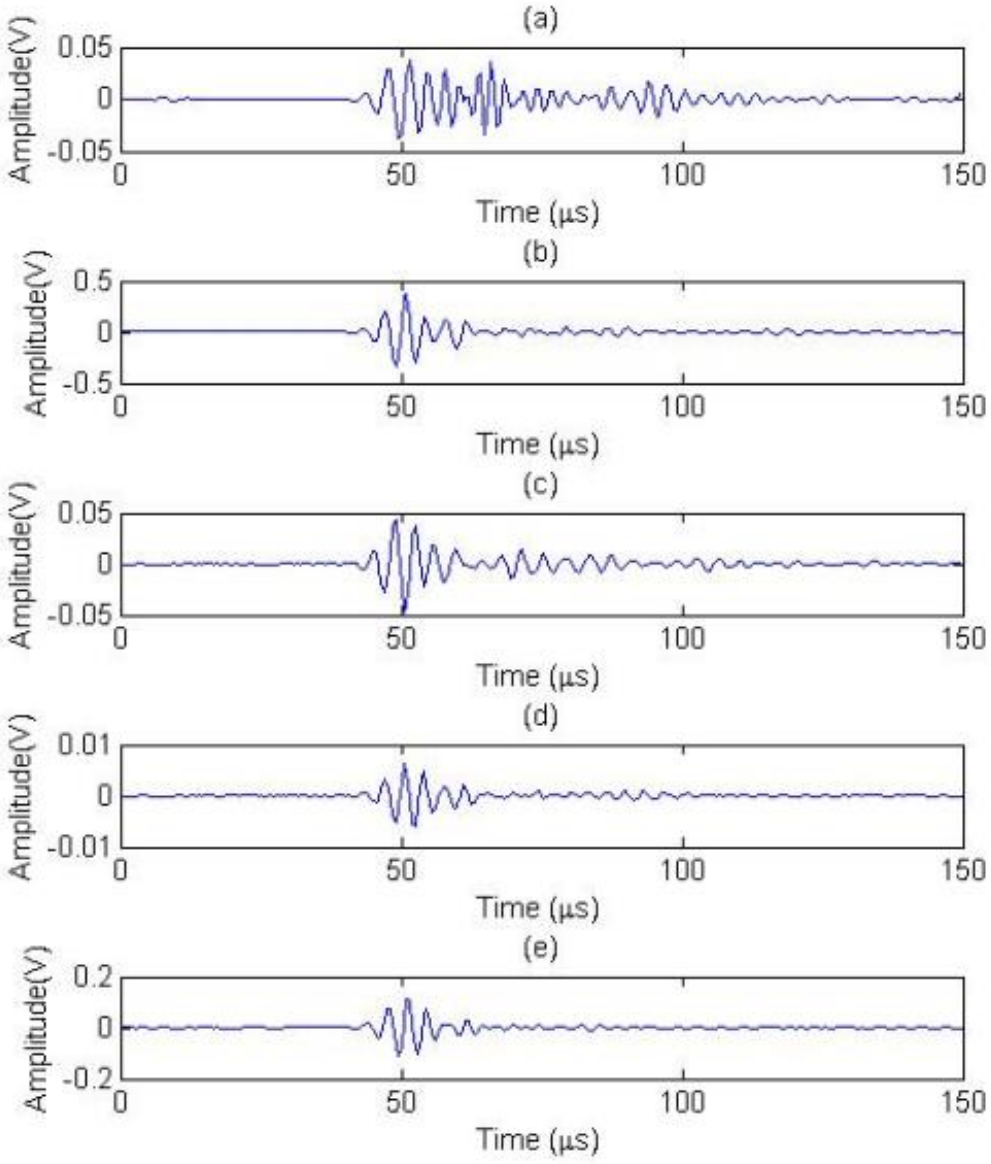

APPENDIX E

TDOA ERROR BAR ON COMPOSITE PLATE FOR ACTIVE TESTING

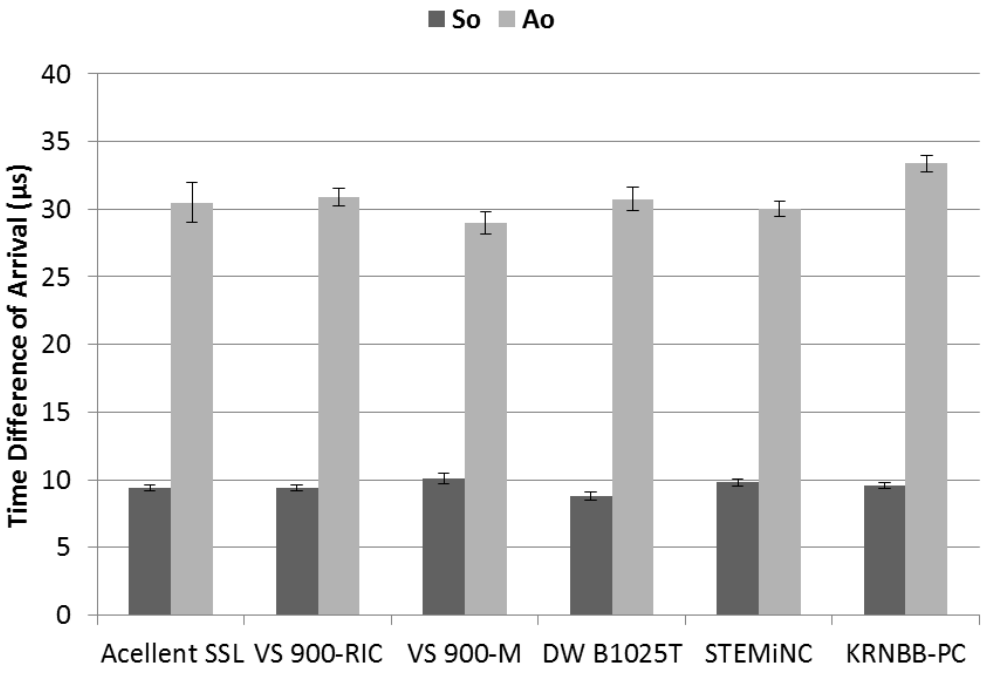

APPENDIX F

STEEL BALL DROP TESTING RESULTS ON ALUMINUM PLATE

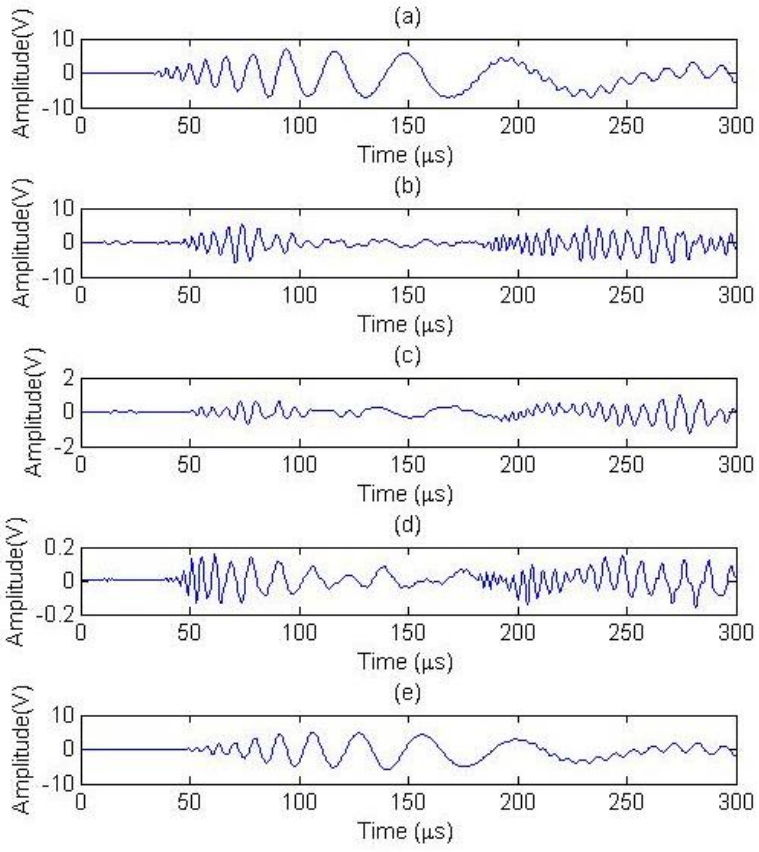

Signal-to-Noise Ratio (SNR):

(a) SNR = 52.35 dB
(b) SNR = 48.20 dB
(c) SNR = 37.44 dB
(d) SNR = 20.50 dB
(e) SNR = 50.00 dB

APPENDIX G

SNR ERROR BAR ON ALUMINUM PLATE FOR STEEL BALL DROP TESTING

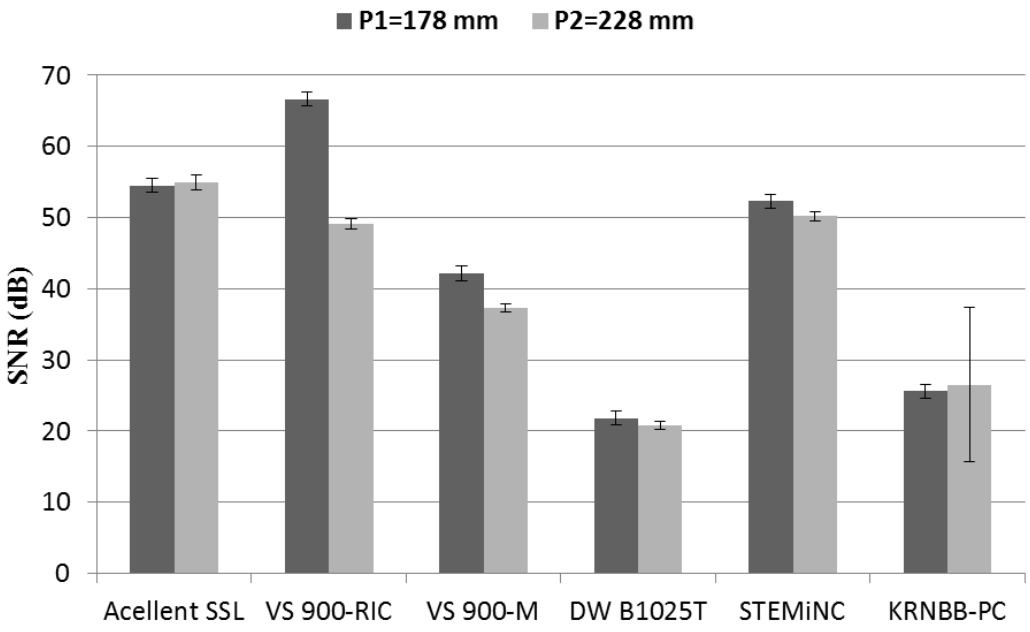

APPENDIX H

IMPACT RESULTS USING EDGE-CLAMPED BOUNDARY CONDITION - IM7/8551

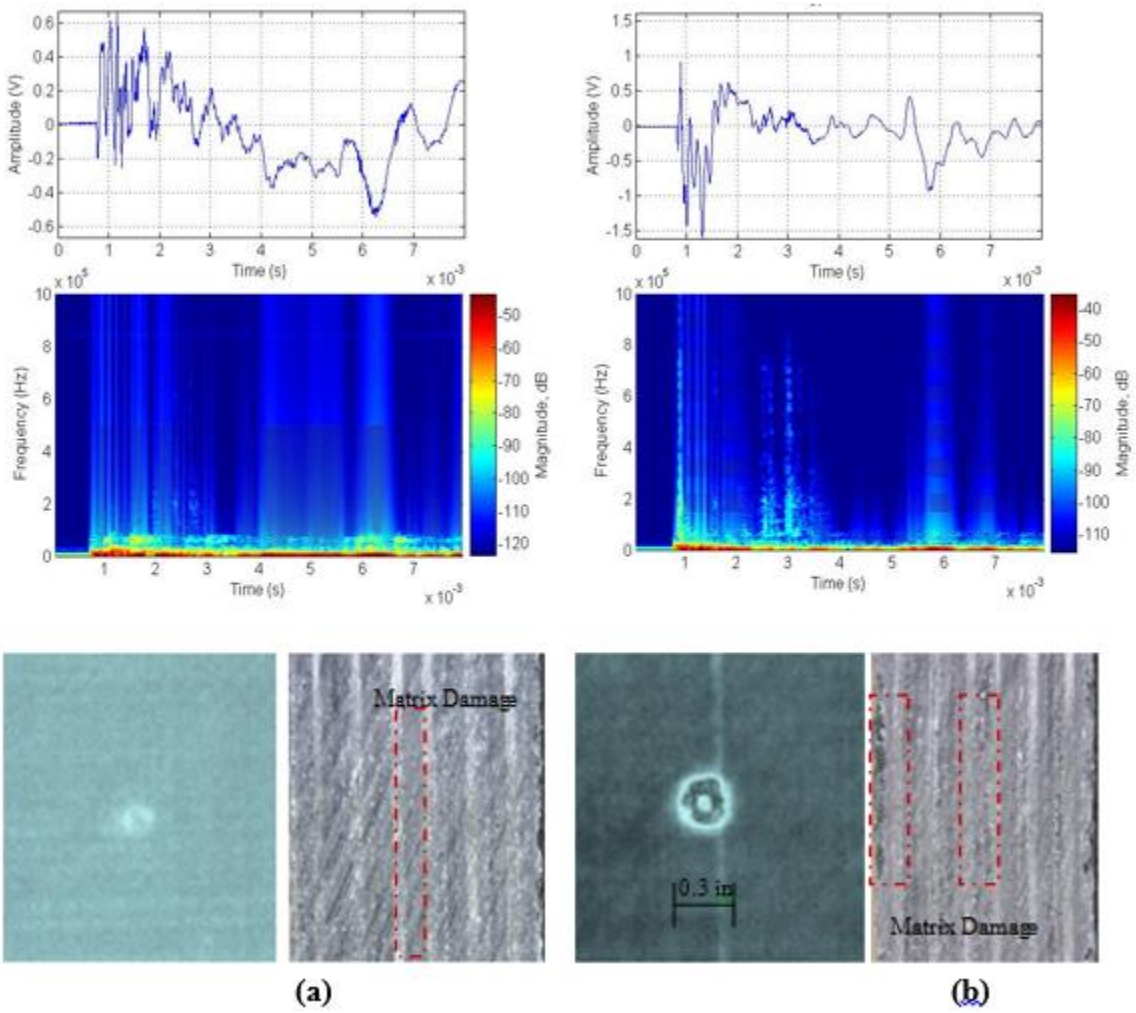

Signal Response, Amplitude Spectrogram and Scan Results for IM7/8551 Material Type Using Impact Energies (a) 3.13 ft-lbf (b) 4.69 ft-lbf.

APPENDIX I

IMPACT RESULTS USING BACK-FACE SUPPORT BOUNDARY CONDITION - IM7/8551

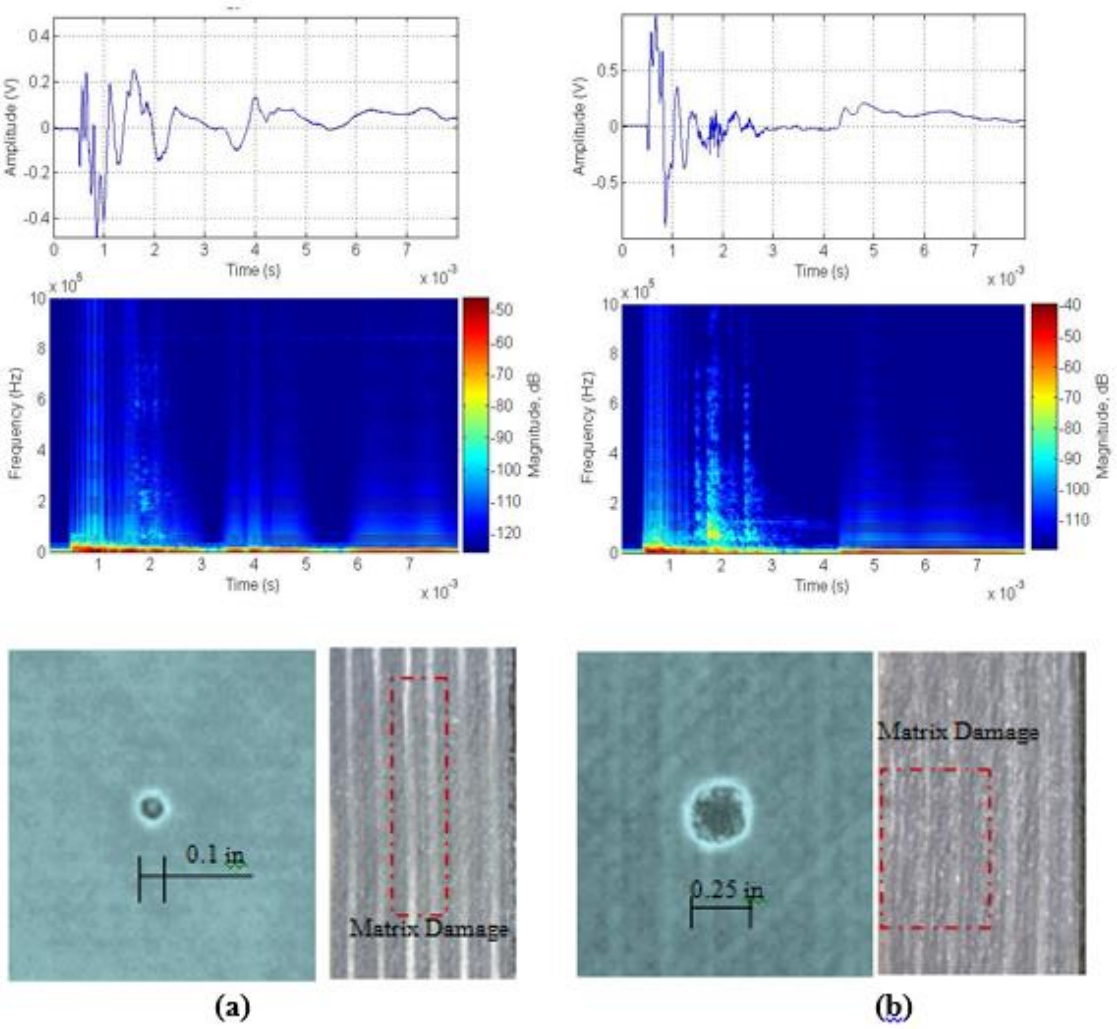

Signal Response, Amplitude Spectrogram and Scan Results for IM7/8551 Material Type Using Impact Energies (a) 1.57 ft-lbf (b) 3.15 ft-lbf.

APPENDIX J

ULTRASONIC C-SCAN TESTING PARAMETERS

J.1 General motor specifications for all testing:

1. Rep rate (Hz) = off
2. Energy = 2
3. Damping = 0
4. Receiver attenuator = 34 dB (have the front follower around 50 FSH so it covers the peak amplitude at all times)
5. Amplifier
    a. Gain = max
    b. Vernier (dB) = 0
    c. Phase inverted = Normal (0°)
6. Filters
    a. Hi pass = 0.5 MHz
    b. Low pass = 75 MHz

J.2 Scan parameters

1. Area scanned : 2 in x 2 in around impact area
2. Number of Gates = 8
    a. AS4/3501 ➔ Each Gate = 0.0156" (three-ply thickness)
    b. IM7/8551 ➔ Each Gate = 0.0168" (three-ply thickness)
    c. IM7/8552 ➔ Each Gate = 0.026" (two-ply thickness)
3. Sampling rate = 100 MHz
4. Axis
    a. Scan Axis = X-Axis
    b. Step Axis = Y-Axis
5. Length
    a. Scan Axis Length = 2.00"
    b. Step Axis Length =2.00"
6. Increment
7. Scan Increment = 0.015"
8. Step Increment = 0.015"
9. Scan Acceleration = 30 in/s2
10. Scan Velocity = 3.5 in/s

APPENDIX K

MAJOR MATLAB SCRIPTS

K.1 File Import

```
%% Imports data from a LabView LVM file
lvm_filename = input('Please input the lvm filename with'''': ');  %
with '', without .lvm  e.g. 'P'
append = input('Select data save file: 0--save in a new file; 1-- save
in an existed file: ');

if append == 0
    mat_filename = input('Please input the new mat filename with'''':
');
else
    mat_filename = input('Please input the existed mat filename
with'''': ');

end

signal_structure = lvm_import(lvm_filename);
eval([lvm_filename,'= signal_structure.Segment1.data',';'])

if append == 0
    save(mat_filename,lvm_filename);
else
    save(mat_filename,lvm_filename,'-append');
end
```

```
%% Import File function
%% Imports data from a LabView LVM file

function data = lvm_import(filename,verbose)

if nargin < 2, verbose = 1; end
if verbose >= 1, fprintf(1,'\nlvm_import v2.1\n'); end
if nargin < 1
    filename=input(' Enter the name of the .lvm file: ','s');
    fprintf(1,'\n');
end
```

```
fid=fopen(filename);
      if fid ~= -1, % then file exists
fclose(fid);
else
    filename=strcat(filename,'.lvm');
    fid=fopen(filename);
    if fid ~= -1, % then file exists
        fclose(fid);
    else
        error(['File not found in current directory! (' pwd ')']);
    end
end

fid=fopen(filename); % open the validated file
if verbose >= 1, fprintf(1,' Importing %s:\n\n',filename); end
if verbose >= 2, fprintf(1,' File Header:\n'); end

% is it really a LVM file?
linein=fgetl(fid);
if verbose >= 2, fprintf(1,'%s\n',linein); end
if ~strcmp(sscanf(linein,'%s'),'LabVIEWMeasurement')
    try
        data.Segment1.data = dlmread(filename,'\t');
        if verbose >= 1, fprintf(1,'This file appears to be an LVM file
with no header.\n'); end
        if verbose >= 1, fprintf(1,'Data was copied, but no other
information is available.\n'); end
        return
    catch fileEx
        error('This does not appear to be a text-format LVM file (no
header).');
    end
end

%% Process file header
data.Decimal_Separator = '.';
text_delimiter='\t';
data.X_Columns='One';

while 1
    linein=fgetl(fid); % get a line from the file
    if isempty(linein), linein=fgetl(fid); end
    if verbose >= 2, fprintf(1,'%s\n',linein); end % tag for the line?
    t_in = textscan(linein,'%s');
    if isempty(t_in{1})
        tag='notag';
    else
        tag = t_in{1}{1};
    end
    if strcmpi(tag,'***End_of_Header***')
        if verbose >= 2, fprintf(1,'\n'); end
        break
    end
    if ~strcmp(tag,'notag')
        v_in = textscan(linein,'%*s %s','delimiter','\t',
            'whitespace','','MultipleDelimsAsOne', 1);
```

```
        if ~isempty(v_in{1})
            val = v_in{1}{1};
                switch tag
                case 'Date'
                    data.Date = val;
                case 'Time'
                    data.Time = val;
                case 'Operator'
                    data.user = val;
                case 'Description'
                    data.Description = val;
                case 'Project'
                    data.Project = val;
                case 'Separator'
                    if strcmp(val,'Tab')
                        text_delimiter='\t';
                    elseif strcmp(val,'Comma')
                        text_delimiter=',';
                    end
                case 'X_Columns'
                    data.X_Columns = val;
                case 'Decimal_Separator'
                    data.Decimal_Separator = val;
            end
         end
    end
end

if isfield(data,'time') && isfield(data,'date')
    dt = textscan(data.Date,'%d','delimiter','/');
    tm = textscan(data.Time,'%d','delimiter',':');
    if length(tm{1})==3
        data.clock=[dt{1}(1) dt{1}(2) dt{1}(3) tm{1}(1) tm{1}(2)
tm{1}(3)];
    elseif length(tm{1})==2
        data.clock=[dt{1}(1) dt{1}(2) dt{1}(3) tm{1}(1) tm{1}(2) 0];
    else
        data.clock=[dt{1}(1) dt{1}(2) dt{1}(3) 0 0 0];
    end
end

% Process segments
segnum = 1;
while 1
    fieldnm = ['Segment' num2str(segnum)];
    if verbose >= 1, fprintf(1,' Segment %d:\n\n',segnum); end
    while 1
        linein=fgetl(fid);
        while isempty(linein), linein=fgetl(fid); end
        if feof(fid), break; end
        if verbose >= 2, fprintf(1,'%s\n',linein); end
        if strfind(linein,'***Start_Special***')
            special_seg = 1;
            while special_seg
                 while 1
                    linein=fgetl(fid);
```

```
                    if isempty(linein), linein=fgetl(fid); end
                    if linein==-1, break; end
                    if verbose >= 2, fprintf(1,'%s\n',linein); end
                    if strfind(linein,'***End_Special***')
                        if verbose >= 2, fprintf(1,'\n'); end
                        break
                    end
                end
                linein=fgetl(fid);
                while isempty(linein), linein=fgetl(fid); end
                if feof(fid), break; end
                if isempty(strfind(linein,'***Start_Special***'))
                    special_seg = 0;
                    if verbose >= 1, fprintf(1,' [Special Segment
              ignored]\n\n'); end
                end
            end
        end % end special segment handler
        t_in = textscan(linein,'%s');
        if isempty(t_in{1})
            tag='notag';
        else
            tag = t_in{1}{1};
        end
        if strcmpi(tag,'***End_of_Header***')
            if verbose >= 2, fprintf(1,'\n'); end
            break
        end
        switch tag
            case 'Notes'
                d_in = linein;
                data.(fieldnm).Notes=d_in;
            case 'Test_Name'
                d_in = linein;
                data.(fieldnm).Test_Name = d_in;  %d_in{1}{1};
            case 'Channels'
                numchan = textscan(linein,'%*s %d',1);
                data.(fieldnm).num_channels = numchan{1};
            case 'Samples'
                numsamp = textscan(linein, '%s', 'delimiter',
                        text_delimiter);
                numsamp1 = numsamp{1};
                numsamp1(1)=[]; % remove tag "Samples"
                numsamp2=str2num(cell2mat(numsamp1));
                data.(fieldnm).num_samples = numsamp2(:)';
            case 'Y_Unit_Label'
                Y_units = textscan(linein,'%s','delimiter',
                  text_delimiter);
                data.(fieldnm).y_units=Y_units{1}';
                data.(fieldnm).y_units(1)=[]; % remove tag
            case 'Y_Dimension'
                Y_Dim = textscan(linein,'%s','delimiter',
                  text_delimiter);
                data.(fieldnm).y_type=Y_Dim{1}';
                data.(fieldnm).y_type(1)=[]; % remove tag
            case 'X_Unit_Label'
```

```
                X_units = textscan(linein,'%s','delimiter',
                  text_delimiter);
                data.(fieldnm).x_units=X_units{1}';
                data.(fieldnm).x_units(1)=[];
            case 'X_Dimension'
                X_Dim = textscan(linein,'%s','delimiter',
                  text_delimiter);
                data.(fieldnm).x_type=X_Dim{1}';
                data.(fieldnm).x_type(1)=[]; % remove tag
            case 'X0'
                [Xnought, val]=strtok(linein);
                if ~strcmp(data.Decimal_Separator,'.')
                    val = strrep(val,data.Decimal_Separator,'.');
                end
                data.(fieldnm).X0 = sscanf(val,'%e');
            case 'Delta_X' %,
                [Delta_X, val]=strtok(linein);
                if ~strcmp(data.Decimal_Separator,'.')
                    val = strrep(val,data.Decimal_Separator,'.');
                end
                data.(fieldnm).Delta_X = sscanf(val,'%e');
        end
    end % end reading segment header loop

    linein=fgetl(fid);
    Y_labels = textscan(linein,'%s','delimiter',text_delimiter);
    data.(fieldnm).column_labels=Y_labels{1}';
    if strcmpi(data.X_Columns,'No')
        data.(fieldnm).column_labels(1)=[];
    end
    if any(strcmpi(data.(fieldnm).column_labels,'Comment'))

data.(fieldnm).column_labels=data.(fieldnm).column_labels(1:find(strcmp
i(data.(fieldnm).column_labels,'Comment'))-1);
    end
    % display column labels
    if verbose >= 1
        fprintf(1,' Data Columns:\n | ');
        for i=1:length(data.(fieldnm).column_labels)
            fprintf(1,'%s | ',data.(fieldnm).column_labels{i});
        end
        fprintf(1,'\n\n');
    end

    if verbose >= 1, fprintf(1,' Importing data from Segment
      %d...',segnum); end
        switch data.X_Columns
        case 'No'
            % an empty X column exists in the file
            numdatacols = data.(fieldnm).num_channels+1;
            xColPlural='no X-Columns';
        case 'One'
            numdatacols = data.(fieldnm).num_channels+1;
            xColPlural='one X-Column';
        case 'Multi'
            numdatacols = data.(fieldnm).num_channels*2;
```

```
            xColPlural='multiple X-Columns';
    end

    if ~strcmp(data.Decimal_Separator,'.')
        if verbose >= 2, fprintf(1,'\n  (using decimal separator
      "%s")\n',data.Decimal_Separator); end
        fs = '%s'; for i=2:numdatacols+1, fs = [fs ' %s']; end
        % read data from file
        rawdata = textscan(fid,fs,'delimiter',text_delimiter);
        % save first row comment as The Comment for this segment
        data.(fieldnm).Comment = rawdata{size(rawdata,2)}{1};
        for i=1:length(rawdata)
            for j=1:length(rawdata{i})
      rawdata{i}(j)=strrep(rawdata{i}(j),data.Decimal_Separator,'.');
            end
            rawdata{i}=str2double(rawdata{i});
        end

    else
        fs = '%f'; for i=2:numdatacols, fs = [fs ' %f']; end
        fs = [fs ' %s'];
        rawdata = textscan(fid,fs,'delimiter',text_delimiter);
        data.(fieldnm).Comment = rawdata{size(rawdata,2)}{1};
    end
    data.(fieldnm).data=rawdata{1};
    for i=2:numdatacols
        data.(fieldnm).data=[data.(fieldnm).data rawdata{i}];
    end
    if strcmpi(data.X_Columns,'No')
        data.(fieldnm).data=data.(fieldnm).data(:,2:end);
    end

    if verbose >= 1, fprintf(1,' complete (%g data
      points).\n\n',length(data.(fieldnm).data)); end

    if isfield(data.(fieldnm),'num_samples')
        if length(data.(fieldnm).data) ~=
      data.(fieldnm).num_samples(1)
            if verbose >= 1
                fprintf(1,' WARNING: Number of data points read in
      segment (%g) is not equal to\n',length(data.(fieldnm).data));
                fprintf(1,'          number of samples shown in the
      segment header (%g)\n\n',data.(fieldnm).num_samples(1));
            end
        end
    end
    if feof(fid)
        if verbose >= 2, fprintf(1,' [End of File]\n\n'); end
        break;
    else
        segnum = segnum+1;
    end
end % end process segment

if verbose >= 1, fprintf(1,' Import complete. File has %s and %d Data
Segments.\n\n',xColPlural,segnum); end
```

```
% close the file
fclose(fid);
return
```

K.2 Signal Average for Active Testing

```
%% Averages multiple signals for active testing condition only

clc
name='test';% Variable define
StartRow =24;
exp_num =  4;
EndRow = 200023;
triger =0.00008;
Data= zeros(EndRow-24,exp_num);

for i= 3:exp_num
    Filename = ['Delam' num2str(i) '.lvm'];
    Data(:,i) = importfile(Filename, StartRow, EndRow);
    Data(:,i) = detrend(Data(:,i));
end

[row_num, col_num] = size(Data);
signal_all = zeros(row_num, col_num, exp_num);

avg = mean(Data,2);
eval([name '=Data;']);
eval(['Avg' name  '=avg;']);
Time = ['time_' name];
[~, t]=min(abs((avg)-triger));
eval([Time '=t;']);
save(name,name,Time,['Avg' name]);
```

```
%% Import file for averaging signals

function Receiver1 = importfile(filename, startRow, endRow)

delimiter = '\t';

if nargin<=2
    startRow = 24;
    endRow = inf;
end

formatSpec = '%*s %f %*s %[^\n\r]'; % 2nd column

fileID = fopen(filename,'r'); % Open the text file.

%% Read columns of data according to format string.

textscan(fileID, '%[^\n\r]', startRow(1)-1, 'ReturnOnError', false);
```

```
dataArray = textscan(fileID, formatSpec, endRow(1)-startRow(1)+1,
'Delimiter', delimiter, 'ReturnOnError', false);
for block=2:length(startRow)
    frewind(fileID);
    textscan(fileID, '%[^\n\r]', startRow(block)-1, 'ReturnOnError',
false);
    dataArrayBlock = textscan(fileID, formatSpec, endRow(block)-
startRow(block)+1, 'Delimiter', delimiter, 'ReturnOnError', false);
    dataArray{1} = [dataArray{1};dataArrayBlock{1}];
end

fclose(fileID); % Close the text file.

%% Create output variable
Receiver1 = [dataArray{1:end-1}];
```

K.3 Fast Fourier Transform

```
%% Performs Fast Fourier Transform on received signal in terms of
magnitude amplitude

Fs = 2e6; % Sampling frequency
L = 200000; % signal length
NFFT = 2^nextpow2(L); % Next power of 2 from length of y
f = Fs/2*linspace(0,1,NFFT/2+1);

a1 =  X6(:,1); % one sensor signal
b1 = fft(a1,NFFT);
c1 = 2*abs(b1(1:NFFT/2+1));

plot(f,mag2db(c1),'b')
hold on;
title('2 inch drop')
xlabel('Frequency (Hz)')
ylabel('Magnitude(dB)')
grid;
```

K.4 Amplitude Spectrogram

```
%% Calculate waveform and amplitude spectrogram of received signal
%% Modified based on Time-Frequency Analysis with MATLAB
Implementation; Authors: M.Sc. Eng. Hristo Zhivomirov, M.Sc. Eng. Kiril
Nenkov

clear all;
clc;
load('BFS.mat')

fs = 2e6;
x =  DWAs44(:, 1); % Input filename
xmax = max(abs(x)); % find the maximum abs value
x = x/xmax; % scaling the signal
```

```
xlen = length(x); % signal length
xdur = xlen/fs; % signal duration
time = (0:xlen-1)/fs; % time scale
wlen = 1024; % window length
h = wlen/4; % hop size
nfft = 2*wlen; % number of fft points
TimeRes = wlen/fs; % time resolution
FreqRes = fs/wlen; % frequency resolution

% time-frequency grid parameters
k = 1+fix((xlen-wlen)/h);           % number of time segments
TimeResGrid = xdur/k;               % time resolution of the grid, s
FreqResGrid = fs/nfft;              % frequency resolution of the grid,
Hz

% define the coherent amplification of the window
K = sum(hamming(wlen, 'periodic'))/wlen;

% perform STFT
[stft, f, t] = stft(x, wlen, h, nfft, fs);

% take the amplitude of fft(x) and scale it, so not to be a
% function of the length of the window and its coherent amplification
SA = abs(stft)/wlen/K;

% correction of the DC & Nyquist component
if rem(nfft, 2)                     % odd nfft excludes Nyquist point
    SA(2:end, :) = SA(2:end, :).*2;
else                                % even nfft includes Nyquist point
    SA(2:end-1, :) = SA(2:end-1, :).*2;
end

% convert the amplitude spectrogram to dB
SA = 20*log10(SA);

time = time';

% plot the signal in time domain
subplot(2,2,1)
plot(time(1:6000,1), x(1:6000,1))
hold on;
grid on
xlim([0 max(time(1:6000,1))])
ylim([-1.1*max(abs(x)) 1.1*max(abs(x))])
xlabel('Time (s)')
ylabel('Amplitude (V)')

% plot the amplitude spectrogram
subplot(2,2,3)
spectrogram(x(1:6000,1),256,224,1024,fs,'yaxis')
set(gca, 'YDir', 'normal')
xlabel('Time (s)')
ylabel('Frequency (Hz)')
```

```
handl = colorbar('East');
climdb(80), handl;
ylabel(handl, 'Magnitude, dB')
set(gcf, 'renderer', 'zbuffer');
```

```
%% Import file to estimate amplitude spectrogram
%% Calculate short time fourier transform
%% Modified based on Short-Time Fourier Transfform with MATLAB
Implementation; Author: M.Sc. Eng. Hristo Zhivomirov

function [stft, f, t] = stft(x, wlen, h, nfft, fs)

if size(x,2) > 1
    x = x';
end

xlen = length(x); % length of the signal
win = hamming(wlen, 'periodic'); % form a periodic hamming window

rown = ceil((1+nfft)/2);% calculate the total number of rows
coln = 1+fix((xlen-wlen)/h); % calculate the total number of columns
stft = zeros(rown, coln);% form the stft matrix

% initialize the indexes
indx = 0;
col = 1;

% perform STFT
while indx + wlen <= xlen
    xw = x(indx+1:indx+wlen).*win; % windowing
    X = fft(xw, nfft);% FFT
    stft(:,col) = X(1:(rown)); % update the stft matrix
    indx = indx + h; % update the indexes
    col = col + 1;
end

% calculate the time and frequency vectors
t = (wlen/2:h:xlen-wlen/2-1)/fs;
f = (0:rown-1)*fs/nfft;
end
```